NACA TN 3675 2868

TECH LIBRARY KAFB, NM
0066381

NATIONAL ADVISORY COMMITTEE FOR AERONAUTICS

TECHNICAL NOTE 3675

THE EFFECTS OF COMPRESSIBILITY ON THE UPWASH AT THE PROPELLER PLANES OF A FOUR-ENGINE TRACTOR AIRPLANE CONFIGURATION HAVING A WING WITH 40° OF SWEEPBACK AND AN ASPECT RATIO OF 10

By Armando E. Lopez and Jerald K. Dickson

Ames Aeronautical Laboratory
Moffett Field, Calif.

Washington
July 1956

TECHNICAL LIBRARY
APL 201

.A

TECH LIBRARY KAFB, NM
0066381

NATIONAL ADVISORY COMMITTEE FOR AERONAUTICS

TECHNICAL NOTE 3675

THE EFFECTS OF COMPRESSIBILITY ON THE UPWASH AT THE PROPELLER PLANES OF A FOUR-ENGINE TRACTOR AIRPLANE CONFIGURATION HAVING A WING WITH 40° OF SWEEPBACK AND AN ASPECT RATIO OF 10[1]

By Armando E. Lopez and Jerald K. Dickson

SUMMARY

An investigation has been conducted in which upflow angles were measured along the horizontal center lines of the propeller planes of a semispan model representing a multiengine airplane with tractor propellers. The wing had 40° of sweepback, an aspect ratio of 10, and a taper ratio of 0.4. Tests were conducted at Reynolds numbers of 2, 4, 6, and 8 million at low Mach numbers, and a Reynolds number of 2 million at Mach numbers from 0.25 to 0.92.

In addition, the upflow was measured with the nacelle alone to evaluate the theoretical method for predicting the upwash induced by the nacelle. The tests with the nacelle alone were conducted at a Reynolds number of 4 million at a Mach number of 0.123, and at a Reynolds number of 2 million at Mach numbers from 0.60 to 0.92.

The results indicate that for Mach numbers up to 0.60 the upwash angles can be predicted accurately by the available theoretical methods. At Mach numbers above 0.60 the experimental values were less than those predicted by theory and this difference increased with increasing Mach number.

INTRODUCTION

An important problem associated with high-speed propeller-driven airplanes is the oscillating aerodynamic loads which impose vibratory stresses on the propellers. Since a large portion of these oscillating aerodynamic loads result from nonuniformity and angularity of the flow entering the

[1]Supersedes NACA RM A53A30a by Armando E. Lopez and Jerald K. Dickson, 1953.

propeller plane, studies have been directed toward an understanding of the factors affecting the air-stream characteristics in this region. It appears, on the basis of the investigation reported in reference 1, that satisfactory estimates of the first-order vibratory stresses in a propeller can be made if the upflow angles along the horizontal center line of the propeller planes are known. Aside from its importance in connection with propeller stress problems, knowledge of these upflow angles is also useful in estimating the magnitude of the propeller normal force in connection with longitudinal-stability analyses. The investigations reported in references 2, 3, and 4 have produced theoretical methods for predicting these upflow angles. However, no previous experimental verification is known for Mach numbers above 0.20.

The investigation was conducted in the Ames 12-foot pressure wind tunnel to measure the upflow angles along the horizontal center lines of the propeller planes of a model representing a multiengine, long-range, high-speed airplane throughout a wide range of subsonic Mach numbers, and to compare the measured rate of change of upwash angle with angle of attack with that predicted by methods of references 2, 3, and 4.

NOTATION

A upflow angle, angle of local flow at the horizontal center line of the propeller plane, measured with respect to the thrust axis in a plane parallel to the plane of symmetry, $\alpha + \epsilon + \gamma$, deg

A_u upflow angle uncorrected for tunnel induced upwash, deg

a mean-line designation, fraction of chord over which design load is uniform

$b/2$ semispan of model, ft

c local chord of wing parallel to plane of symmetry, ft

c' wing chord perpendicular to the reference sweep line, ft

C_L lift coefficient, lift/qS

c_{l_i} design section lift coefficient

M free-stream Mach number

q free-stream dynamic pressure, $\frac{1}{2}\rho V^2$, lb/sq ft

R Reynolds number based on the mean aerodynamic chord of the wing

r_o propeller radius, ft

r/r_o fraction of propeller radius

r_1 spinner radius, ft
(See fig 1(c).)

r_2 nacelle radius, ft
(See fig 1(c).)

S area of semispan wing, sq ft

t maximum thickness of section, ft

V free-stream velocity, ft/sec

y lateral distance from plane of symmetry, ft

α angle of attack of wing chord at the plane of symmetry, deg

α_g geometric angle of attack, angle between tunnel center line and wing chord at the plane of symmetry, deg

γ nacelle inclination, angle between the root chord and the projection of the thrust axis on the plane of symmetry, positive nose up, deg

ϵ angle of upwash, angle of local flow measured with respect to the free-stream direction in a plane parallel to the plane of symmetry, deg

η fraction of semispan

ρ mass density of air in free stream, slugs/cu ft

φ angle of wing twist (positive for washin) measured in a plane parallel to the plane of symmetry, deg

$\frac{\partial\epsilon}{\partial\alpha}$ upwash parameter, rate of change of upwash with angle of attack

MODEL AND APPARATUS

The geometry of the wind-tunnel model is shown in figure 1 and table I. The selection of the geometric properties and the details of construction of the wing, fuselage, and upper-surface fences have been discussed in reference 5. The details of the nacelle installation will

be discussed herein only insofar as they are appropriate to the problem of the present investigation. In this regard, the inclination of the thrust axis, with respect to the wing chord, is an important factor since it affects the upflow angle for a given lift coefficient and thus the forces exciting the first-order vibratory stresses in the propeller. By proper selection of the angle of inclination of the thrust axis with respect to the wing chord, the positive upflow angles induced at the low-speed high-gross-weight condition result in excitation forces equal in magnitude to those resulting from the negative upflow angles at the high-speed low-gross-weight condition. (See ref. 2.) For the speed range of a modern high-performance airplane, this inclination of the thrust axis will result in about zero excitation for the design cruise condition.

In accordance with the theoretical method described in appendix B of reference 2, the inclincation of the nacelles was selected to provide zero upflow at the design cruise condition ($C_L = 0.40$, $M = 0.83$). The resulting nacelle arrangement is shown in figure 1(c).

The upflow angles at the horizontal center line of the propeller planes were measured with a 0.312-diameter cylindrical probe shown in the schematic diagram of figure 2. The probe had six pairs of orifices at radii corresponding to 40, 70, and 95 percent of the propeller radius. The probe was operated as a null instrument; that is, the probe was rotated about its axis to the position where the pressures at the two orifices were equal. The angular position of the probe was indicated as a counter reading by the response of an instrument reacting to the displacement of the differential transformer attached to the probe actuating mechanism. Static calibration of the instrument indicated that the angular displacement of the probe could be determined with an accuracy of $\pm 0.03^{\circ}$.

In addition to the static calibration, it was necessary to establish the angular position of the probe for zero upflow angle of each pair of orifices. This was accomplished with the probe and spinner mounted in a uniform stream at zero angle of attack. With the counter reading for zero upflow angle thus established, the counter readings for balanced pressures across each pair of orifices obtained in the tests with the probe mounted on the complete model (fig. 3(a)) and on the nacelle alone (fig. 3(b)) could be interpreted in terms of upflow angle by means of the static calibration.

The estimated over-all accuracy of the upflow angle measurements is $\pm 0.2^{\circ}$ for the tests at the lowest dynamic pressure and $\pm 0.1^{\circ}$ at the highest dynamic pressure.

CORRECTION TO DATA

Complete Model

The corrections to data for tunnel-wall interference resulting from lift on the model were evaluated by the method described in reference 6. The corrected angle of attack was

$$\alpha = \alpha_g + 0.377\ C_L$$

This correction to the angle of attack, which was used only for the lift data presented in figure 4, is based upon the tunnel-induced upwash at the quarter-chord line of the wing. Since the tunnel induced upwash at the propeller planes was not equal to that at the quarter-chord line of the wing, a correction to the total upflow angle was calculated by the method described in reference 6 and was used in the data presented in figures 5 and 6. The correction to the total upflow angle differed little for each propeller plane and was essentially unaffected by a change in Mach number. The corrected angle of upflow was

$$A = A_u - 0.270\ C_L$$

When the measured angle of upflow is corrected for tunnel-induced upwash as is done herein, the angle of attack corresponding to the corrected angle of upflow is the geometric angle of attack of the model in the wind tunnel. As a result, the angles of attack identified in figure 5 are not the same as the angles of attack shown in figure 4, but the data of both figures have been corrected to free-air conditions within the accuracy of the theoretical methods.

The dynamic pressure and the Mach number were corrected for constriction due to the presence of the tunnel walls by the methods of reference 7. These corrections were not modified to allow for the effects of sweep. The corrections to the dynamic pressures and the corresponding corrections to the Mach numbers are listed in the following table:

Corrected Mach number	Uncorrected Mach number	$\frac{q_{corrected}}{q_{uncorrected}}$
0.123	0.123	1.005
.165	.165	1.005
.25	.249	1.005
.60	.597	1.008
.80	.791	1.015
.86	.845	1.021
.90	.877	1.027
.92	.893	1.032

To provide an indication of the influence of the probe on the flow about the model, the measured total lift on the model with the probe installed alternately on each nacelle was compared with similar data obtained for the model with the probe removed. The results of these force measurements are presented in figure 4. It is indicated that the probe caused no significant change in lift coefficient. Since the wing contribution to upwash angle is determined by the lift coefficient, no correction for the effects of the probe was considered necessary.

Isolated Nacelle

The dynamic pressure and the Mach number for the tests on the isolated nacelle were also corrected for constriction due to the presence of the tunnel walls by the method of reference 7. The corrections to the dynamic pressures and corresponding corrections to Mach numbers were:

Corrected Mach number	Uncorrected Mach number	$\frac{q_{corrected}}{q_{uncorrected}}$
0.123	0.123	1.001
.600	.600	1.001
.700	.699	1.002
.800	.798	1.002
.860	.857	1.003
.900	.895	1.005
.920	.914	1.007

DISCUSSION

The measured upflow angles with respect to the thrust axes at various angles of attack of the model are presented in figure 5.

By definition the upflow angle is

$$A = \alpha + \epsilon + \gamma$$

The nacelle inclination was -6.5° for the inner nacelle and -7.0° for the outer nacelle (fig. 1(c)). By use of these values, the measured upflow angles shown in figure 5 may be converted to upwash angles with respect to the free-stream direction for the corresponding angles of attack. Curves of the upwash angle versus angle of attack were essentially linear in the range of angles for which the lift curve of the model was linear. It is apparent from the preceding relationship that a satisfactory theoretical method for predicting the rate of change of upflow angle with angle of attack where the lift curve is linear is one which provides a satisfactory estimate of the rate of change of upwash angle with angle of attack. For convenience, the correlation between theoretical and experimental results will be made using this parameter.

Theoretical Methods

The investigation reported in reference 4 has shown that a theoretical method involving the algebraic addition of the contributions of each component (wing, nacelles, and fuselage) to determine the total upwash provides results which are in good agreement with experimental results obtained at low Mach numbers. This procedure was retained throughout the present analyses.

The contribution of the wing alone was calculated by two theoretical methods. Both these methods are based upon lifting-line theory; both take into account the wing sweep and include a correction for the effects of compressibility by the method outlined in reference 2.

The first method for calculating the contribution of the wing to the upwash is described in appendix A of reference 2 and in reference 3. In reference 2, a procedure is given for predicting the upwash ahead of the wing in the extended wing-chord plane. This method is extended in reference 3 to permit computation of the upwash at points above or below the extended wing-chord plane, expressed as a percentage of that predicted for the corresponding point in the extended wing-chord plane.

The second method for computing the upwash due to the wing assumes a finite number of elemental rectangular vortices distributed spanwise along the quarter-chord line of the wing (ref. 8). The Biot-Savart law was employed to determine the upwash at the propeller plane due to each of the vortices.

These two methods produced results which differed by less than the experimental accuracy. By the use of these methods the upwash was calculated as a function of lift coefficient. The calculated values of $\partial\epsilon/\partial C_L$ were then multiplied by the lift-curve slope to calculate the rate of change of upwash with angle of attack $\partial\epsilon/\partial\alpha$.

The contribution of the nacelles and fuselage to the upwash were calculated by the theoretical method described in the appendix of reference 4. It was assumed that the nacelles and the fuselage were infinite cylinders downstream of their maximum thicknesses. The upwash contributions of the nacelles and fuselage were considered to be independent of Mach number.

Comparison of Experimental and Theoretical Results

Shown in figure 6 are the experimental and the theoretical spanwise variations of the upwash parameter $\partial\epsilon/\partial\alpha$ at a few selected Mach numbers. From the data shown in this figure it is evident that the theoretical methods accurately predicted the spanwise variation and the magnitude of the upwash parameter for Mach numbers of 0.60 or less. Although the theory still predicted the spanwise variation of upwash to a fair degree of accuracy at the higher Mach numbers, it failed to predict the magnitude correctly.

Upwash ahead of the isolated nacelle.- To determine whether the failure of the theoretical method to predict the upwash at the higher Mach numbers was due to the deficiency of the theory as applied to the nacelle and the fuselage, the upflow angles were measured for the isolated nacelle. The results are shown in figure 7. The small upflow angle measured at 0° angle of attack of the thrust axis is assumed to be caused by the asymmetry of the nacelle aft of the propeller plane. The swept strut which supported the nacelle was far enough behind the propeller plane so that, theoretically, its contribution to the upwash was insignificant. This is confirmed by the symmetry of the measured upflow on either side of the nacelle.

Figure 8 shows the variation with Mach number of the upwash parameter $\partial\epsilon/\partial\alpha$ for the nacelle alone at the three radial stations corresponding to 40-, 70-, and 95-percent propeller radius. It is evident

from these data that the nacelle-induced upwash is not independent of Mach number as is assumed in the theoretical method.

Effects of Mach number on upwash.- The variation with Mach number of the upwash parameter $\partial\epsilon/\partial\alpha$ for the complete model is shown in figure 9 for the stations corresponding to 70 percent of the propeller radius. It is indicated that the difference between experimental and theoretical values at Mach numbers above 0.60 increased with increasing Mach number until at a Mach number of 0.92 the predicted values were about twice the measured values.

Figure 9 also indicates that using the experimental values of the nacelle-induced upwash in place of the theoretical values markedly reduced the difference between the predicted and measured values for the complete model. Since the effect of compressibility on the nacelle-induced upwash varied with radial distance from the thrust axis (fig. 8), it was not considered feasible to attempt to apply a correction to the theoretical values of upwash at radial stations other than those at which experimental data were available. It is evident, however, from inspection of figures 6 and 9 that a reduction with increasing Mach number of the fuselage-induced upwash at the inner propeller plane and of the upwash induced by the inner nacelle at the outer propeller plane would result in closer agreement between the measured and computed upwash of the complete model.

It should be noted that while the predicted values of the upwash parameter are about twice as great as the experimental values at a Mach number of 0.92, the theoretical values of the rate of change of the upflow angle with the angle of attack $\partial A/\partial\alpha$ are only about 20 or 30 percent in excess of the measured values. This results from the fact that the geometric angle of attack of the thrust axis accounts for more than three-quarters of the total upflow at high subsonic Mach numbers. This point is emphasized since vibratory stresses on a propeller are computed on the basis of the total upflow angle.

CONCLUDING REMARKS

The present investigation has produced experimental data on the upwash at the propeller planes of a four-engine tractor airplane configuration with a 40° swept-back wing for a range of Mach numbers up to 0.92. Comparisons of the rate of change of upwash angle with angle of attack by the use of the available theoretical methods with those measured in the wind tunnel indicated good agreement up to a Mach number of 0.60. At higher Mach numbers, the predicted values exceeded the experimental values by an amount which increased with increasing Mach number.

It is evident that this discrepancy between the experimental and theoretical results is due, at least in part, to the failure of the theoretical methods to account properly for the effects of compressibility on the upwash induced by the nacelle and fuselage.

Ames Aeronautical Laboratory
National Advisory Committee for Aeronautics
Moffett Field, Calif., Jan. 30, 1953

REFERENCES

1. Roberts, John C., and Yaggy, Paul F.: A Survey of the Flow at the Plane of the Propeller of a Twin-Engine Airplane. NACA TN 2192, 1950.

2. Rogallo, Vernon L.: Effects of Wing Sweep on the Upwash at the Propeller Planes of Multiengine Airplanes. NACA TN 2795, 1952.

3. Rogallo, Vernon L., and McCloud, John L., III: Calculations of Upwash in the Region Above or Below the Wing-Chord Planes of Swept-Back Wing-Fuselage-Nacelle Combinations. NACA TN 2894, 1953.

4. Yaggy, Paul F.: A Method for Predicting the Upwash Angles Induced at the Propeller Plane of a Combination of Bodies With an Unswept Wing. NACA TN 2528, 1951.

5. Edwards, George G., Tinling, Bruce E., and Ackerman, Arthur C.: The Longitudinal Characteristics at Mach Numbers up to 0.92 of a Cambered and Twisted Wing Having 40° of Sweepback and an Aspect Ratio of 10. NACA RM A52F18, 1952.

6. Sivells, James C., and Salmi, Rachel M.: Jet-Boundary Corrections for Complete and Semispan Swept Wings in Closed Circular Wind Tunnels. NACA TN 2454, 1951.

7. Herriot, John G.: Blockage Corrections for Three-Dimensional-Flow Closed-Throat Wind Tunnels, with Consideration of the Effect of Compressibility. NACA Rep. 995, 1950. (Supersedes NACA RM A7B28)

8. Diederich, Franklin W.: Charts and Tables for Use in Calculation of Downwash of Wings of Arbitrary Plan Form. NACA TN 2353, 1951.

TABLE I.- GEOMETRIC PROPERTIES OF THE MODEL

Wing (Reference sweep line: Quarter chord of the sections inclined 40° to the plane of symmetry)		
Aspect ratio		10.0
Taper ratio		0.4
Sweepback		40°
Twist (washout at tip)		5°
Reference sections (normal to reference sweep line)		
Root	NACA 0014, a=0.8 (modified)	$c_{l_i} = 0.4$
Tip	NACA 0011, a=0.8 (modified)	$c_{l_i} = 0.4$
Area (semispan model)		6.944 ft²
Mean areodynamic chord		1.251 ft
Nacelles		
Inclination with respect to root chord reference plane		
Inner nacelle		-6.5°
Outer nacelle		-7.0°
Coordinates		See fig. 1(c)
Propeller		
Radius		7 in.

TABLE I.- CONCLUDED

Fuselage

Fineness ratio 12.6

Fuselage coordinates:

Distance from nose, inches	Radius inches
0	0
1.27	1.04
2.54	1.57
5.08	2.35
10.16	3.36
20.31	4.44
30.47	4.90
39.44	5.00
70.00	5.00
76.00	4.96
82.00	4.83
88.00	4.61
94.00	4.27
100.00	3.77
106.00	3.04
126.00	0

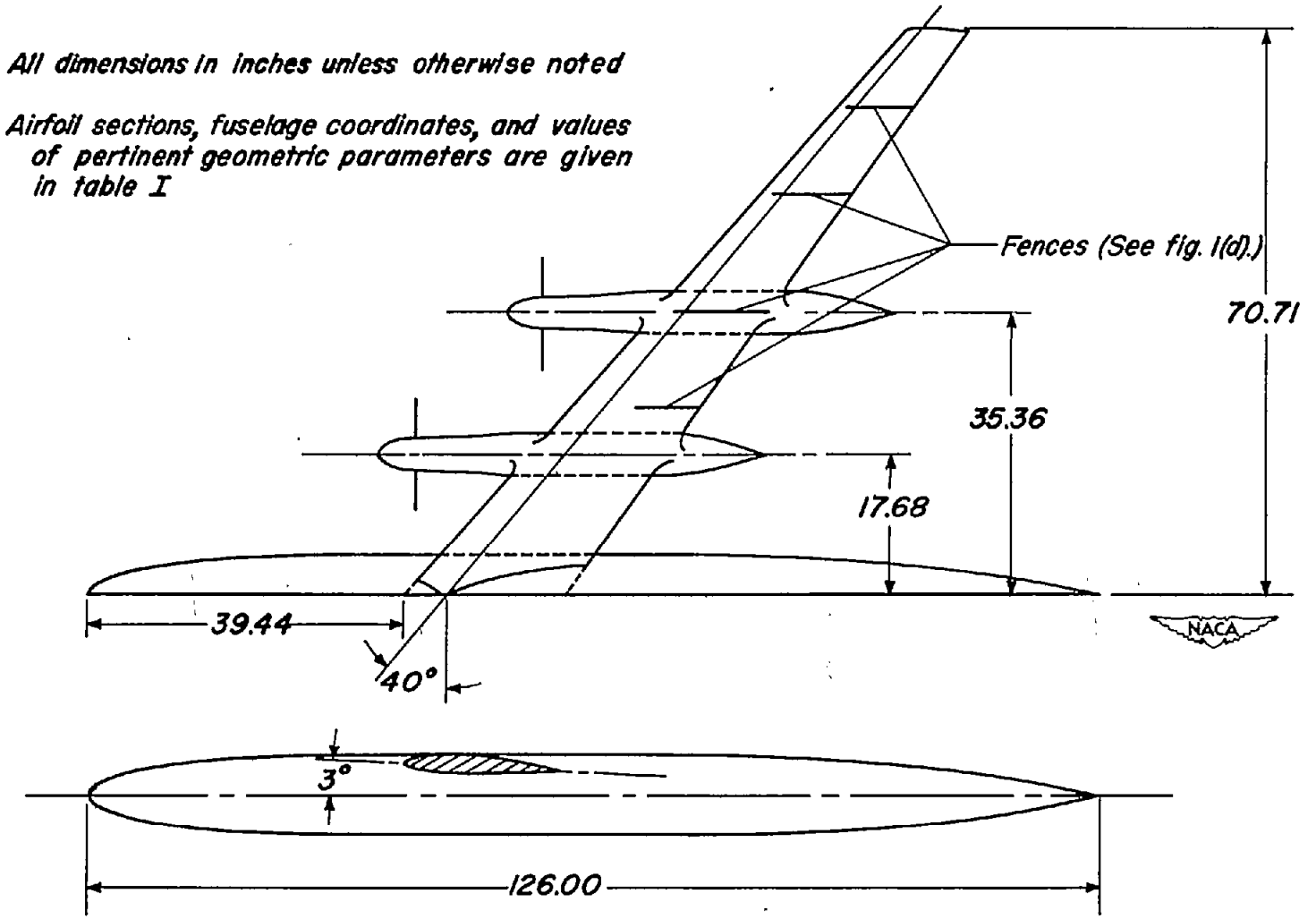

(a) Dimensions.

Figure 1.–Geometry of model.

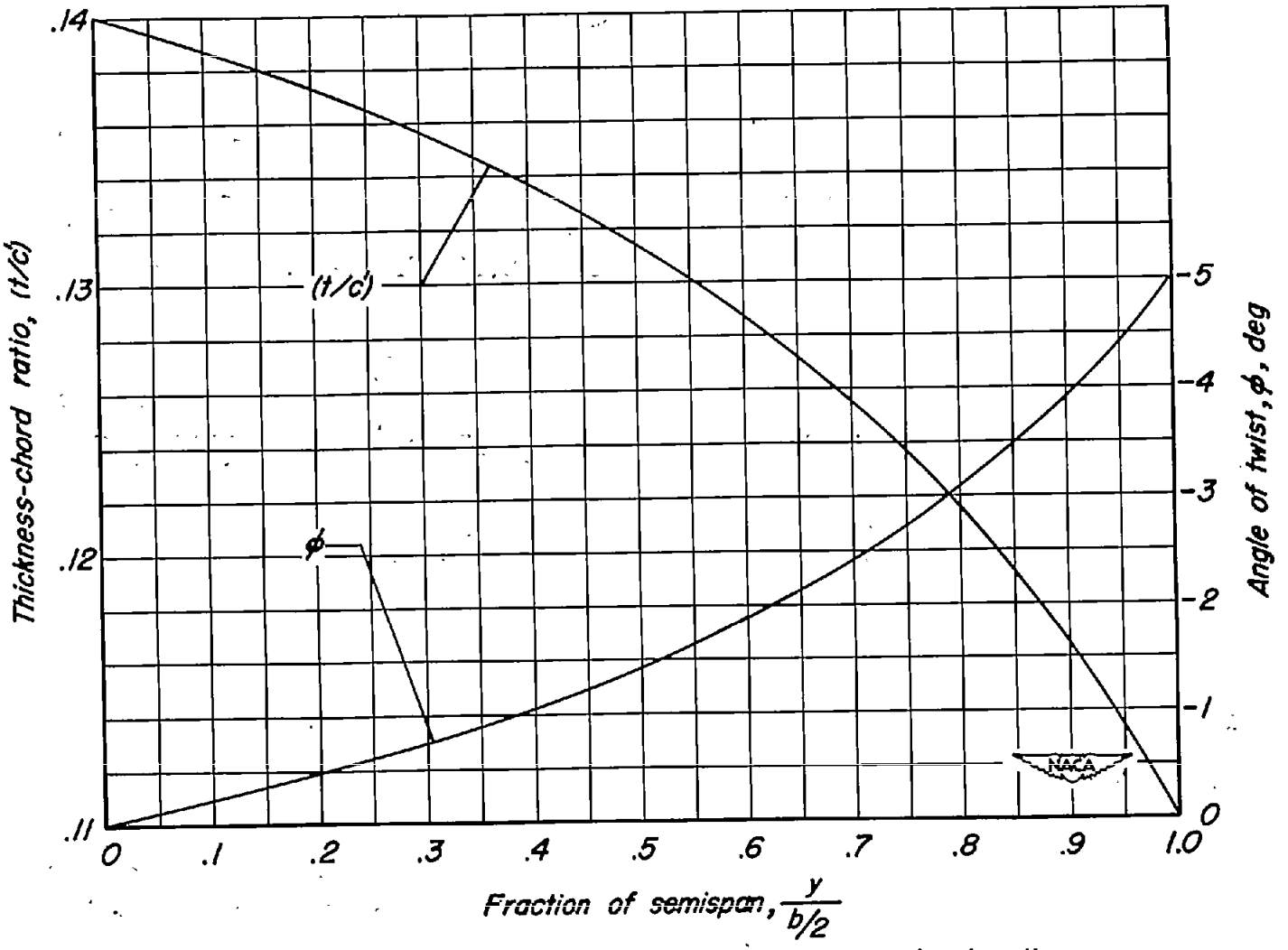

(b) Distribution of wing twist and thickness-chord ratio.

Figure 1.— Continued.

All dimensions are in inches unless otherwise noted.

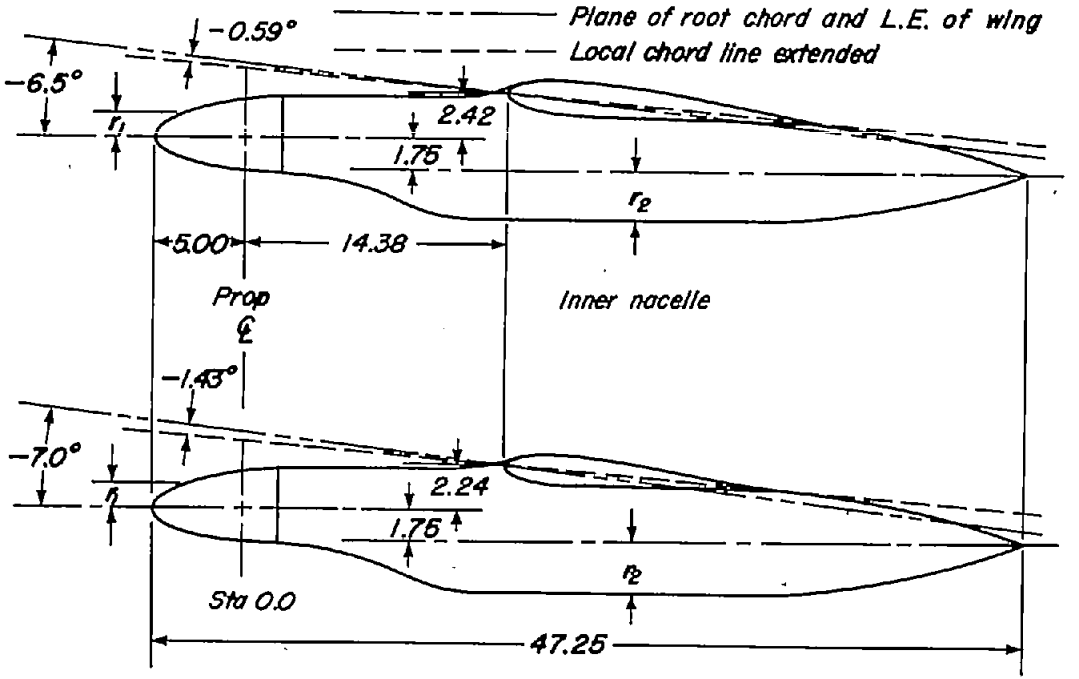

Nacelle coordinates

Sta	r_1	Sta	r_2
-5.00	0	2.00	0.350
-4.79	.385	3.00	.419
-4.58	.567	4.00	.616
-4.25	.788	5.00	.919
-3.95	.951	6.00	1.290
-3.25	1.242	7.00	1.685
-2.55	1.472	8.00	2.056
-1.80	1.670	9.00	2.359
-.80	1.871	10.00	2.556
0	1.985	11.00	2.625
2.00	2.100	30.50	2.625
12.00	2.100	32.50	2.450
		34.50	2.220
		36.50	1.825
		38.50	1.270
		40.50	.675
		41.50	.275
		42.25	0

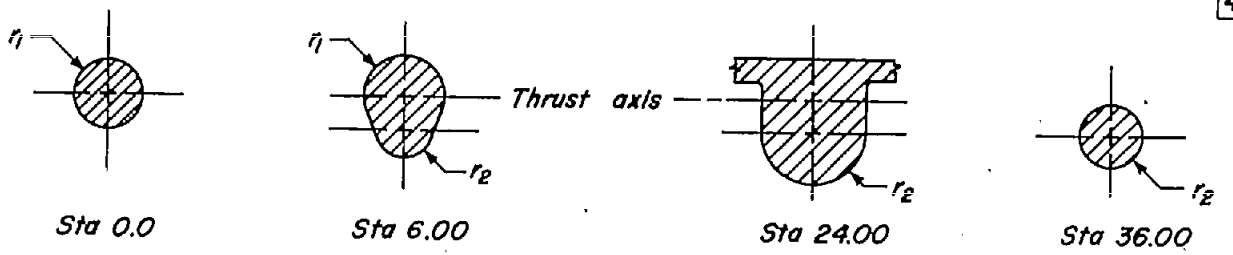

(c) Dimensions of nacelles.

Figure 1.— Continued.

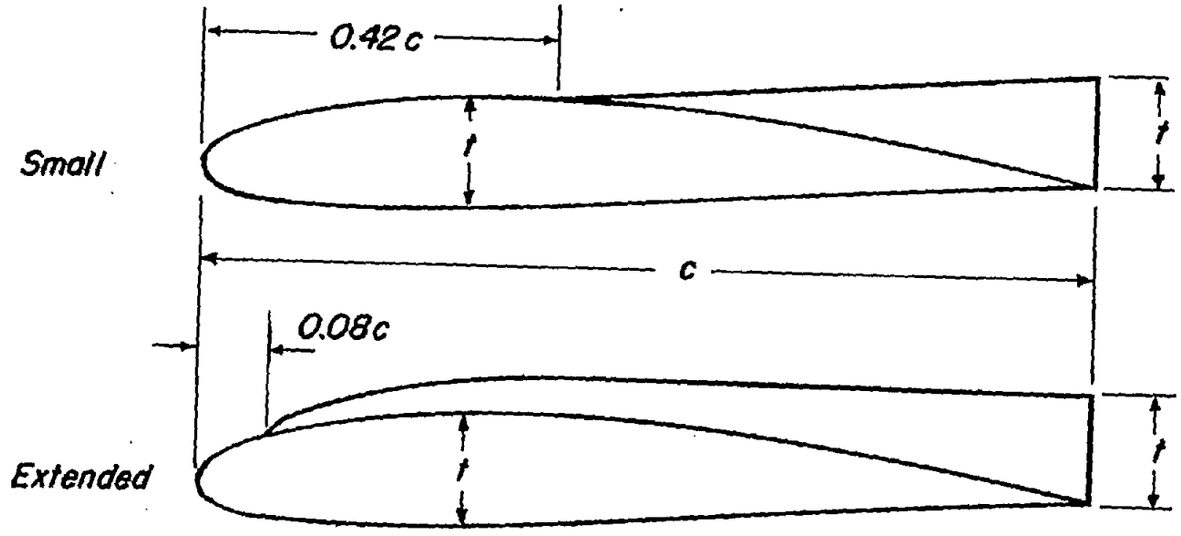

Configuration	Type and location
Four fences	Small at $\frac{y}{b/2} = 0.33$
	Extended at $\frac{y}{b/2} = 0.50, 0.70,$ and 0.85

(d) Fence details.

Figure 1.— Concluded.

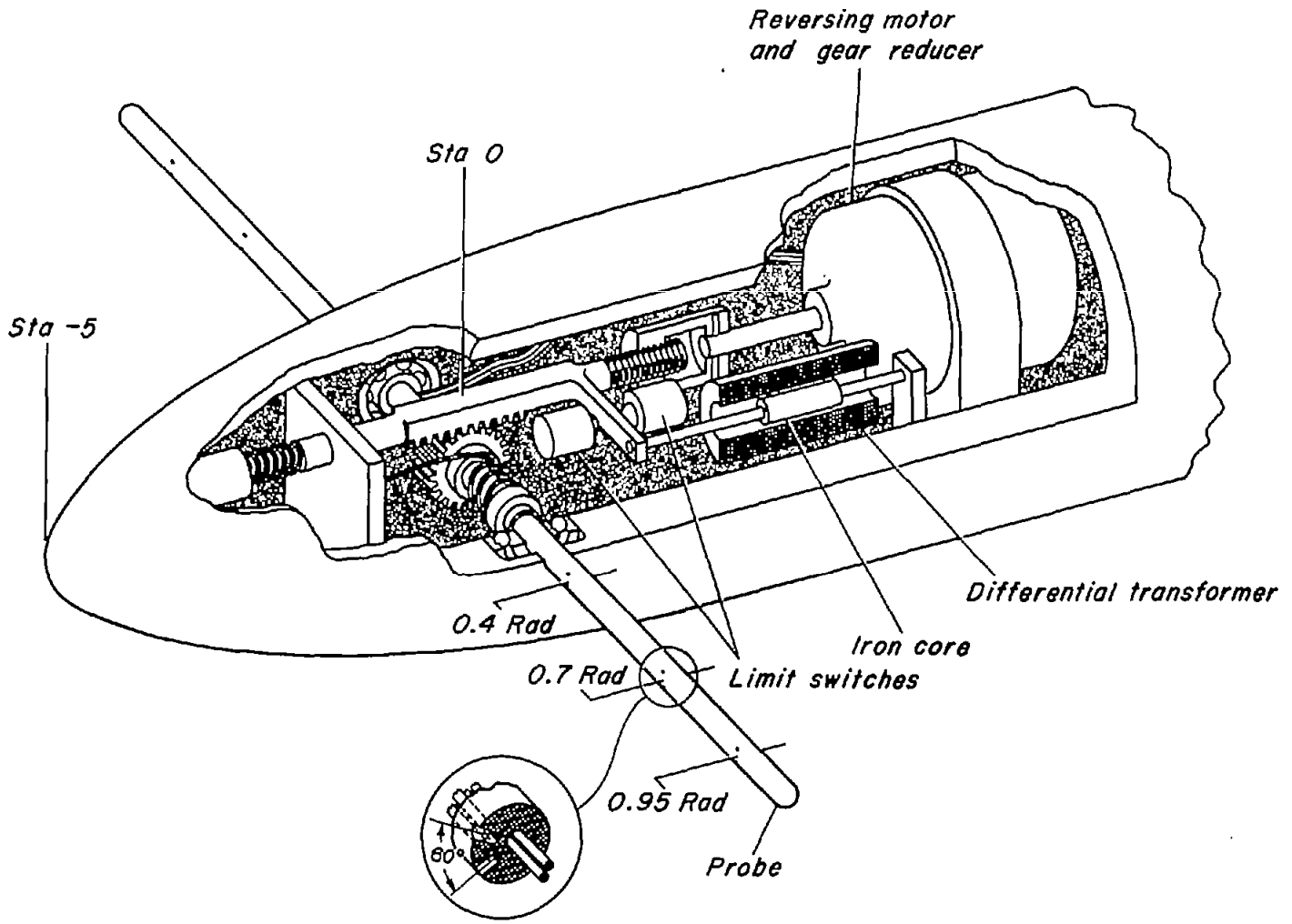

Figure 2.- Schematic drawing of the probe assembly.

NACA
A-17548

(a) The complete model with the probe installed on the inner nacelle.

Figure 3.- Photographs of the models.

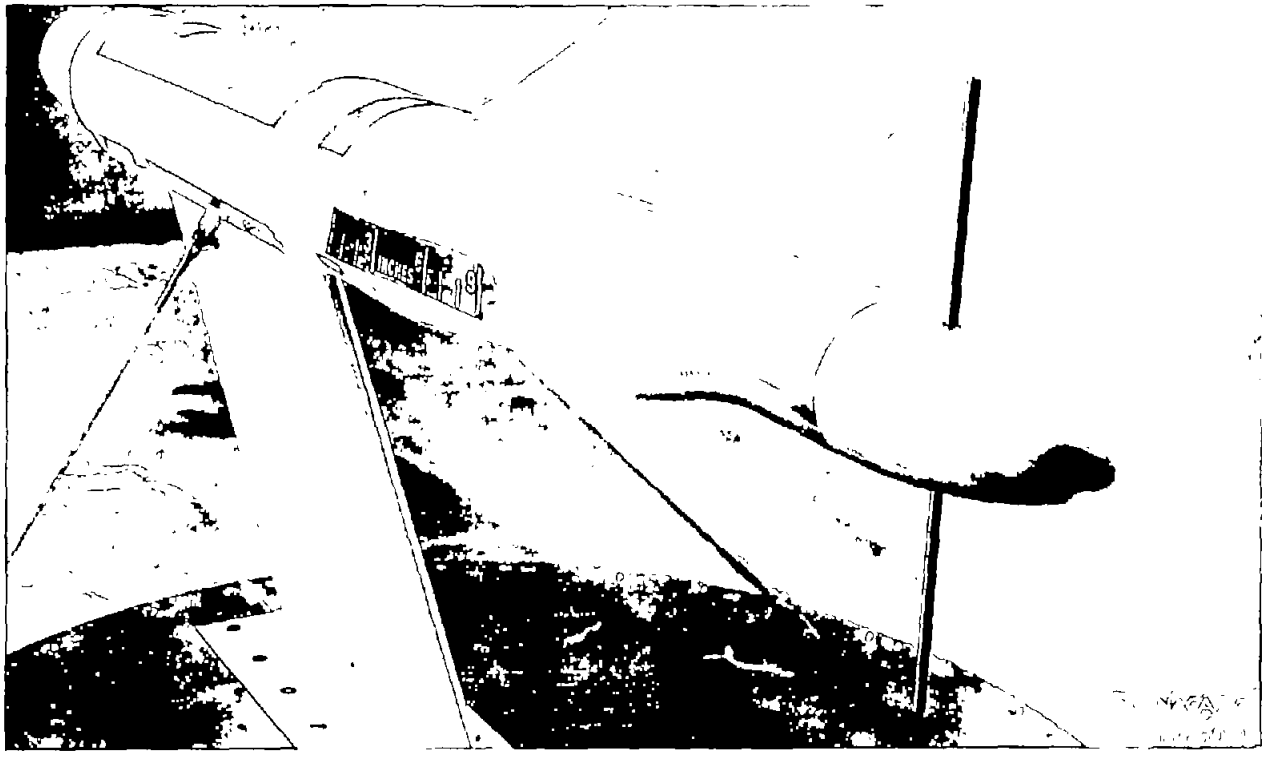

(b) The isolated nacelle with the probe installed.

Figure 3.- Concluded.

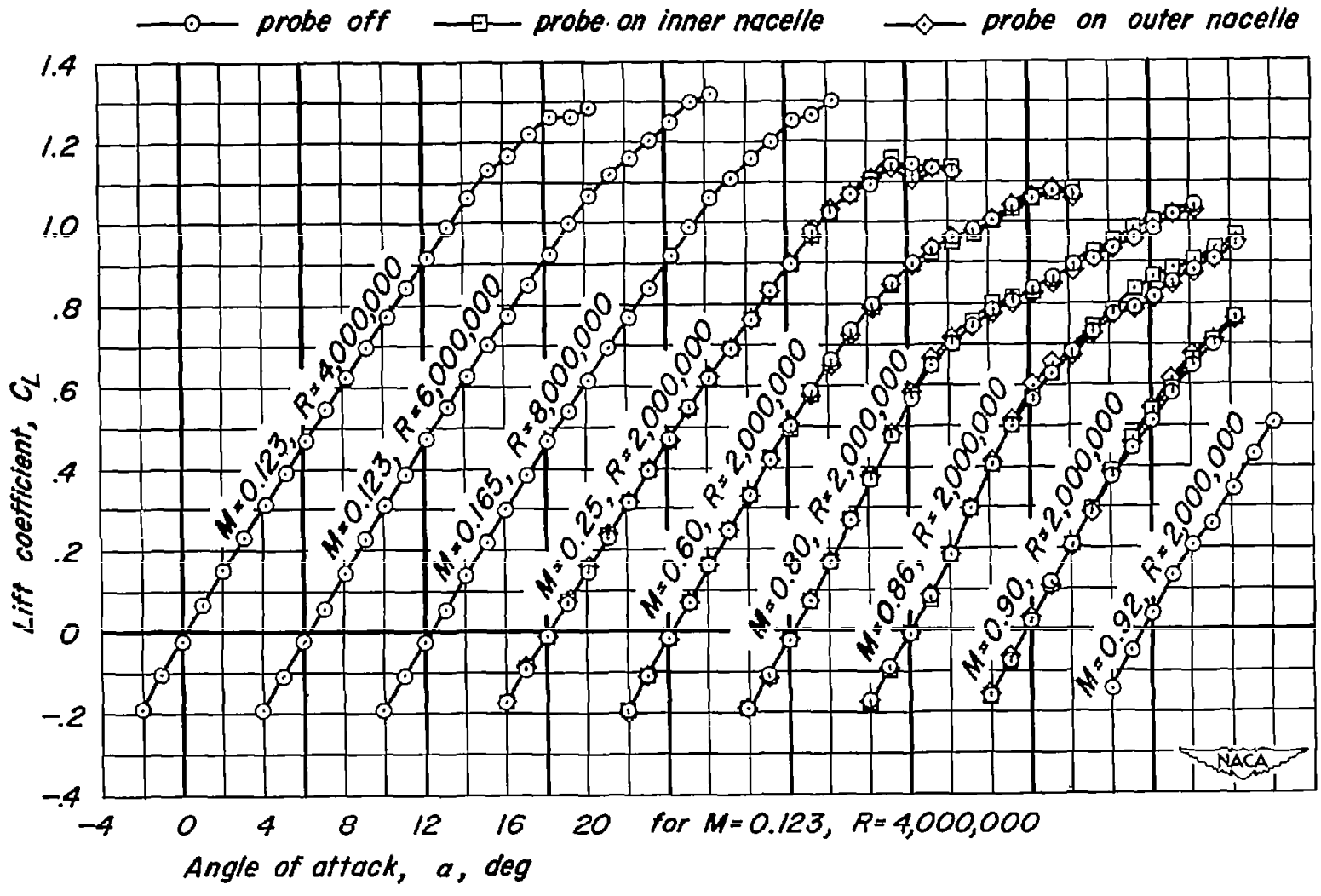

Figure 4.— Variation of lift coefficient with angle of attack.

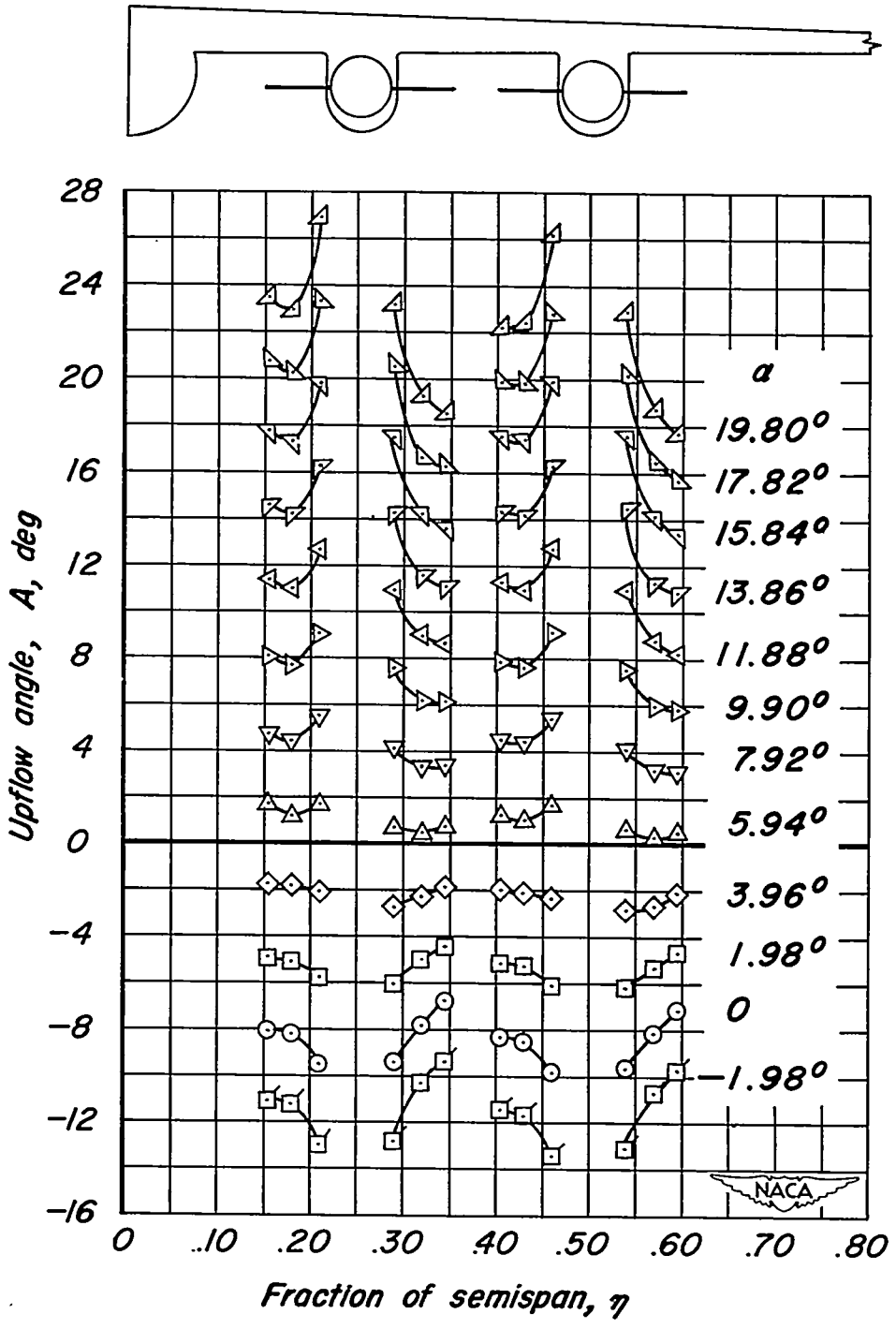

(a) M = 0.123, R = 4,000,000

Figure 5.–Upfow angles at various angles of attack.

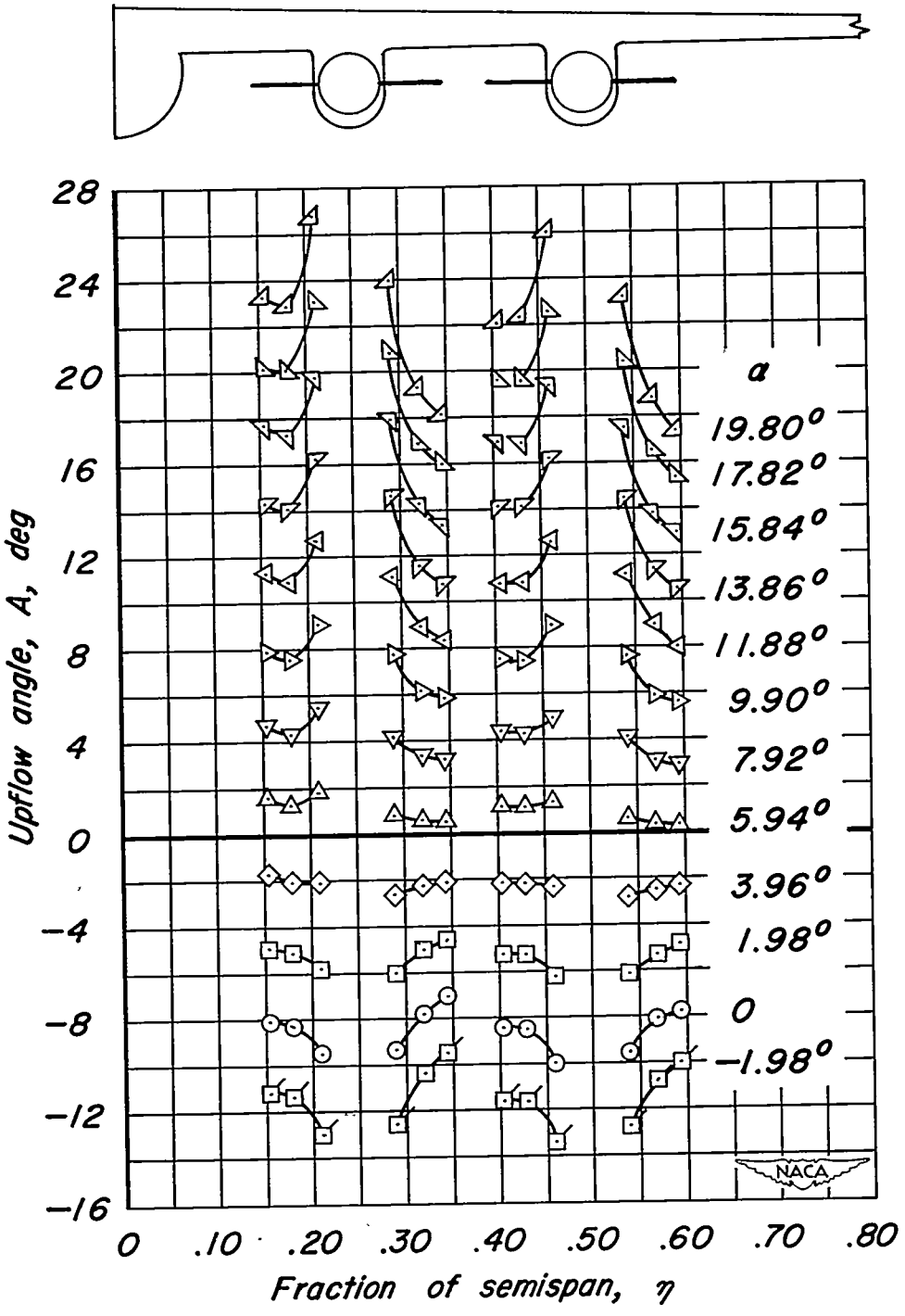

(b) M = 0.123, R = 6,000,000

Figure 5.– Continued.

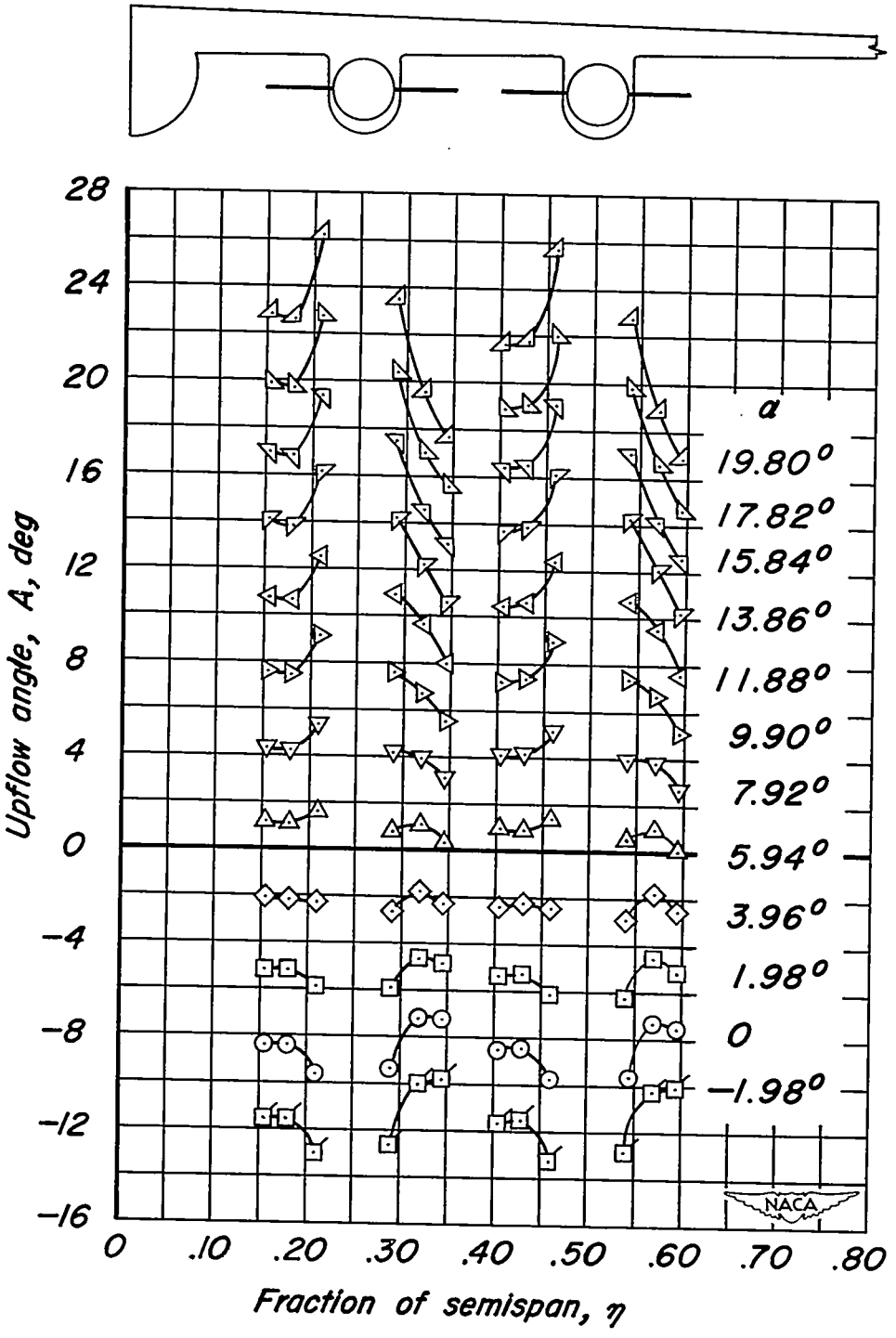

(c) M = 0.165, R = 8,000,000

Figure 5.- Continued.

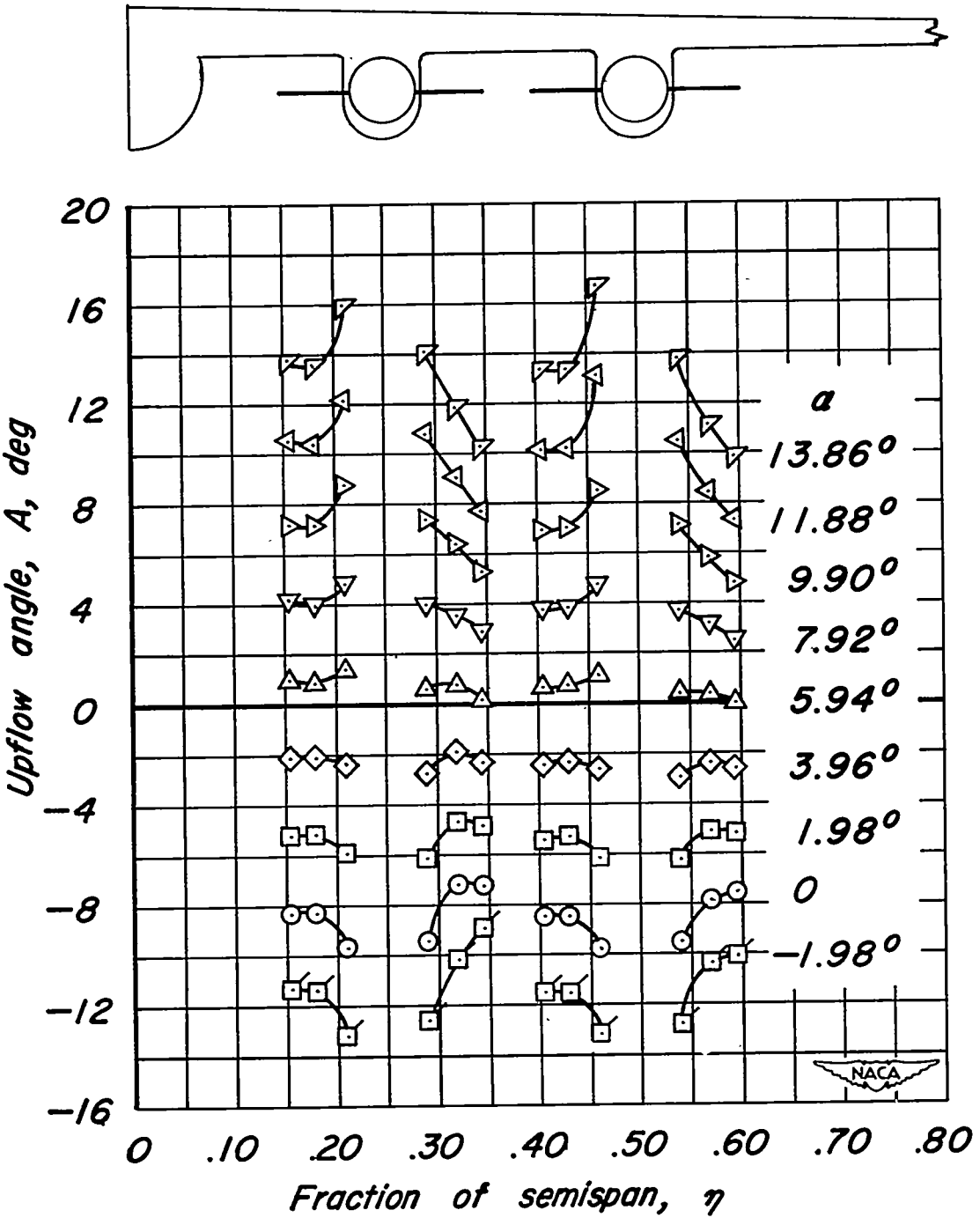

(d) M=0.25, R=8,000,000

Figure 5.– Continued.

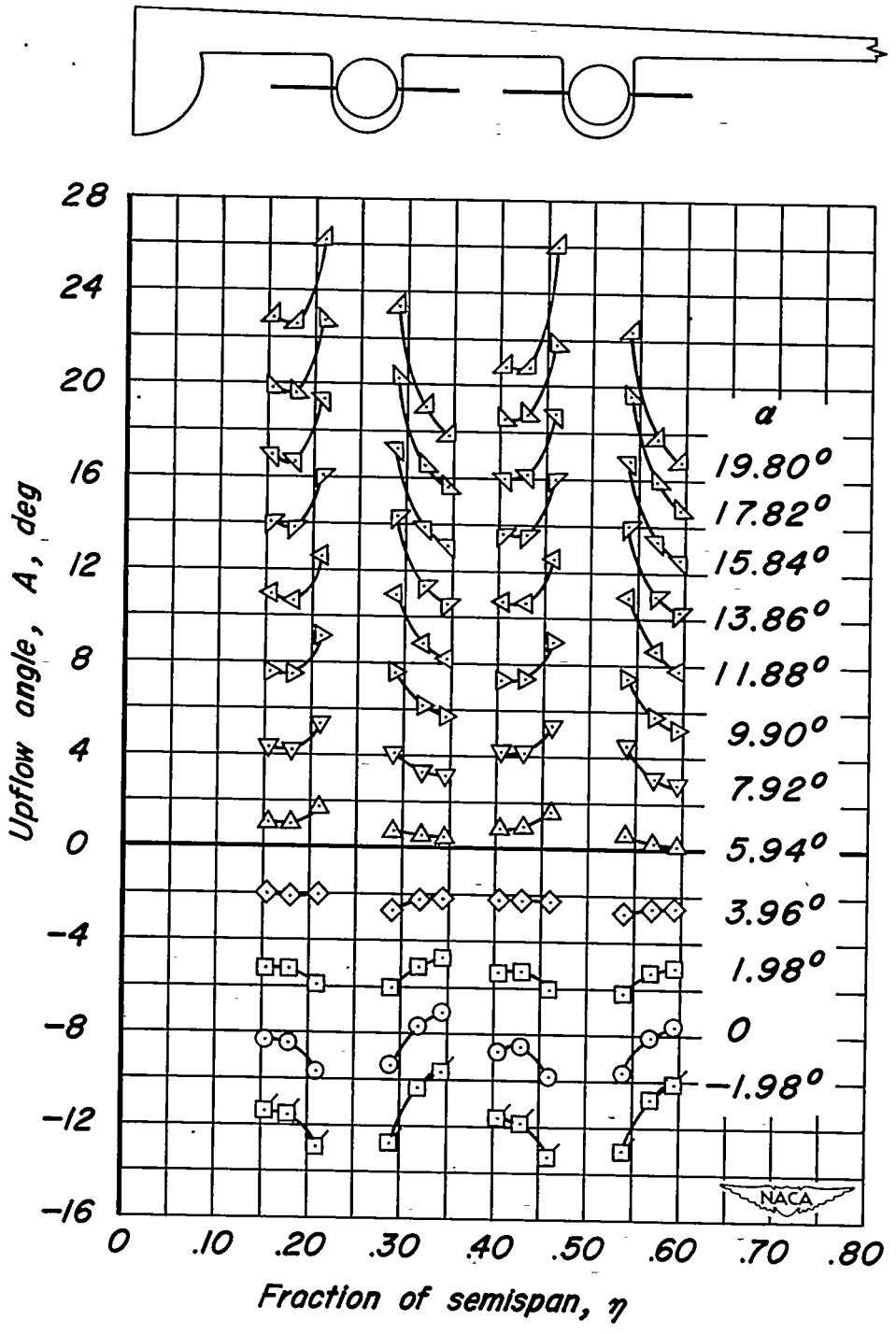

(e) M = 0.25, R = 2,000,000

Figure 5.- Continued.

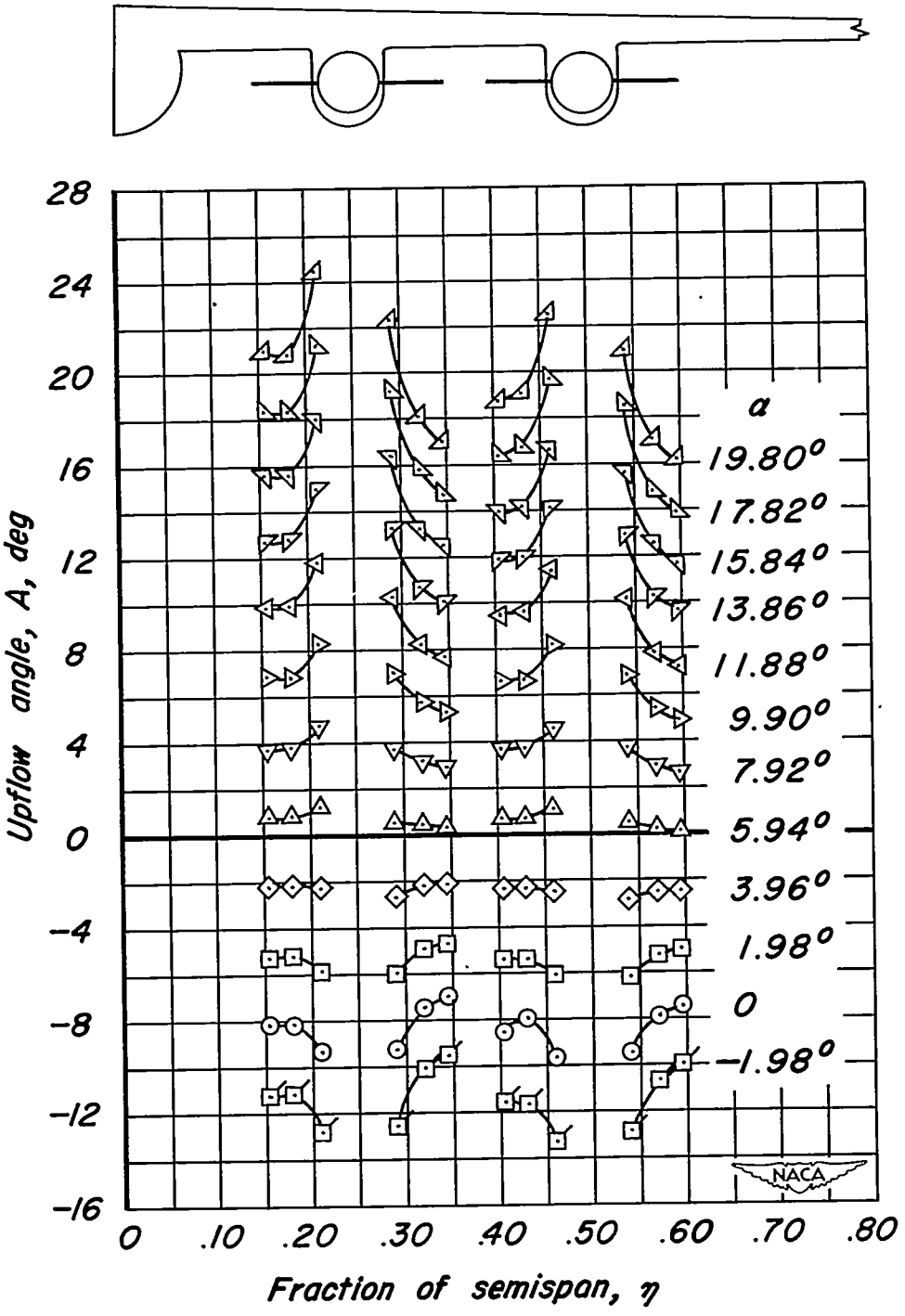

(f) M = 0.60, R = 2,000,000

Figure 5.- Continued.

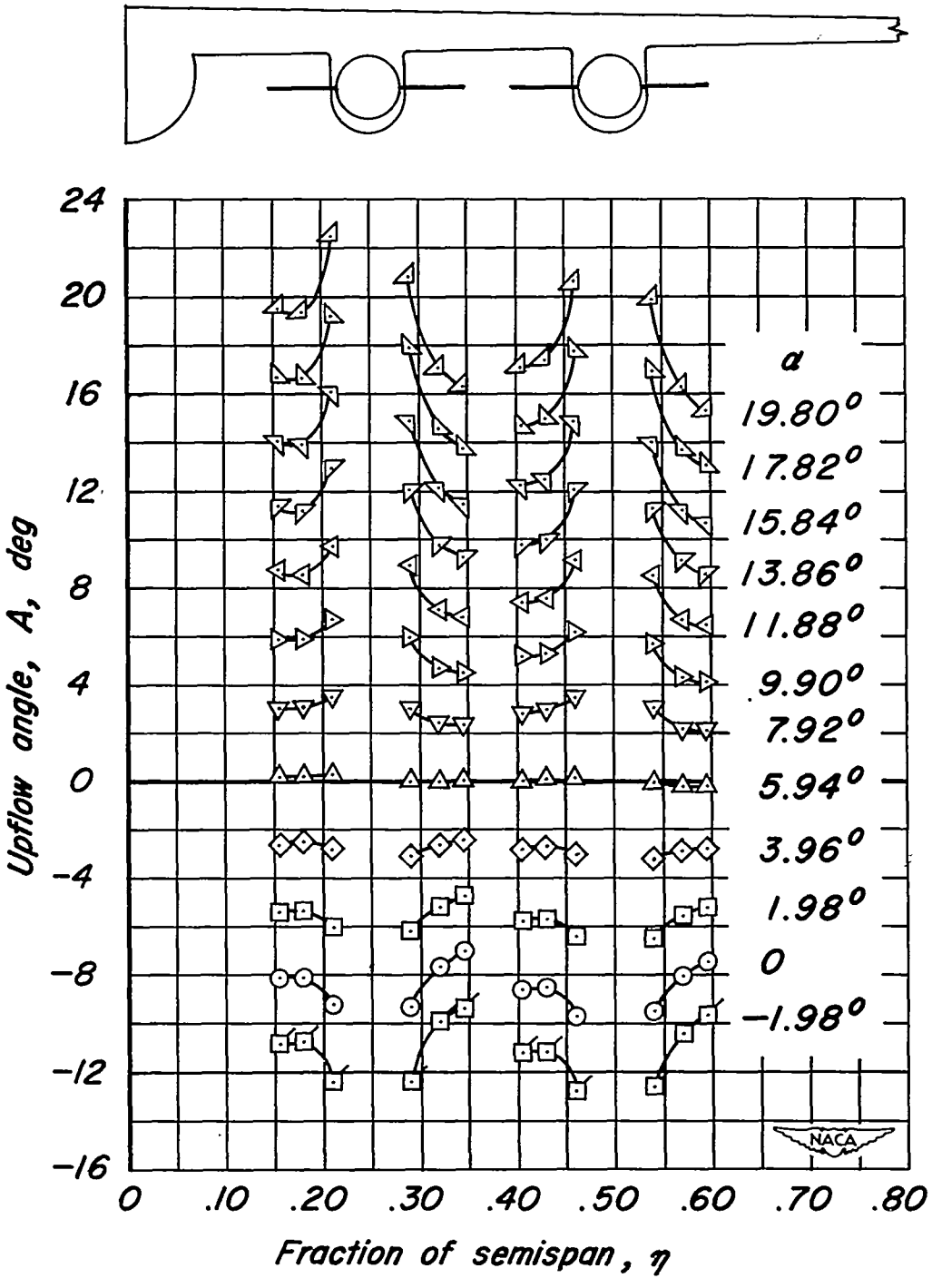

(g) M = 0.80, R = 2,000,000

Figure 5.- Continued.

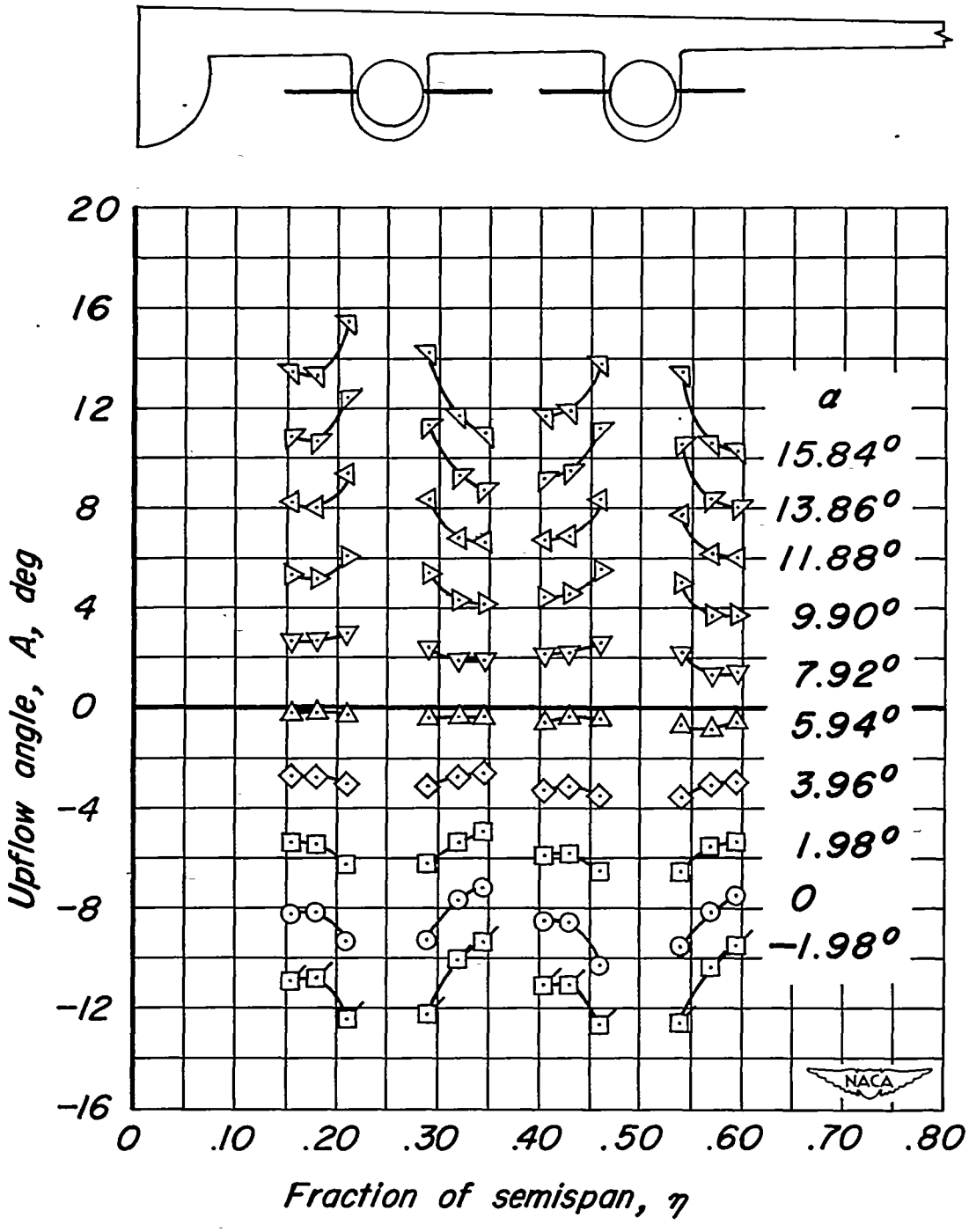

(h) M = 0.86, R = 2,000,000

Figure 5.- Continued.

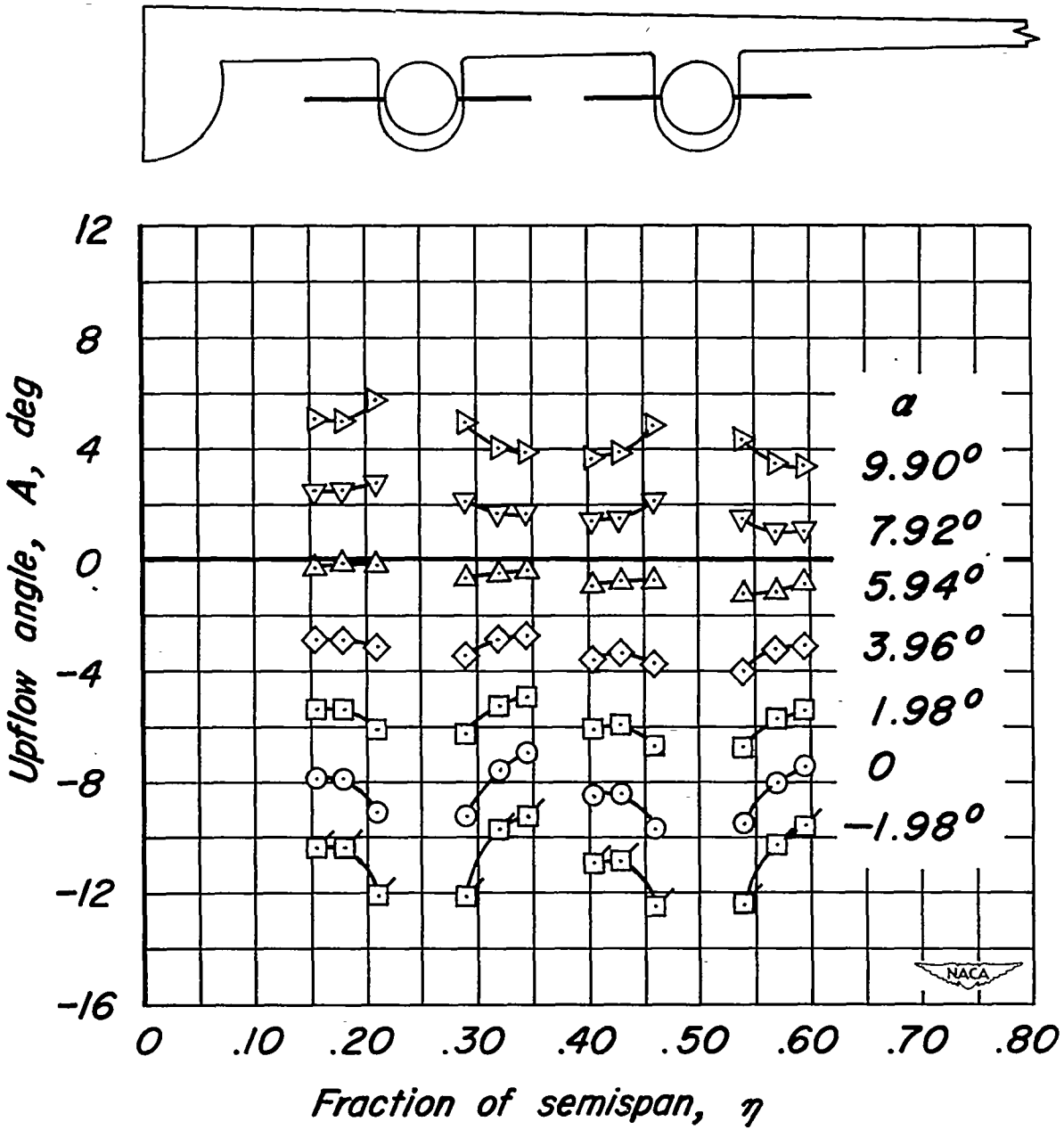

(i) M = 0.90, R = 2,000,000

Figure 5.- Continued.

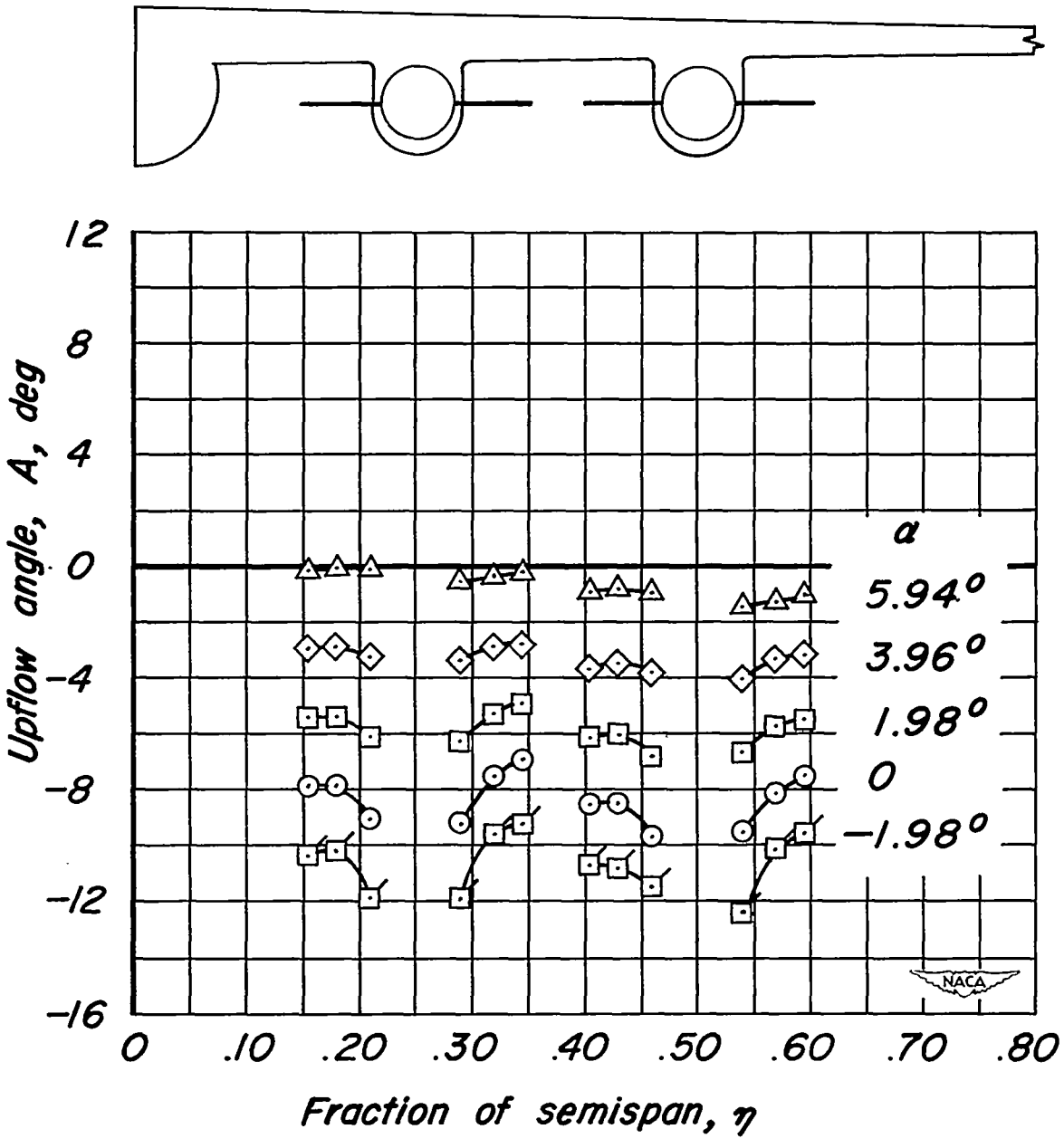

(j) M = 0.92, R = 2,000,000

Figure 5.– Concluded.

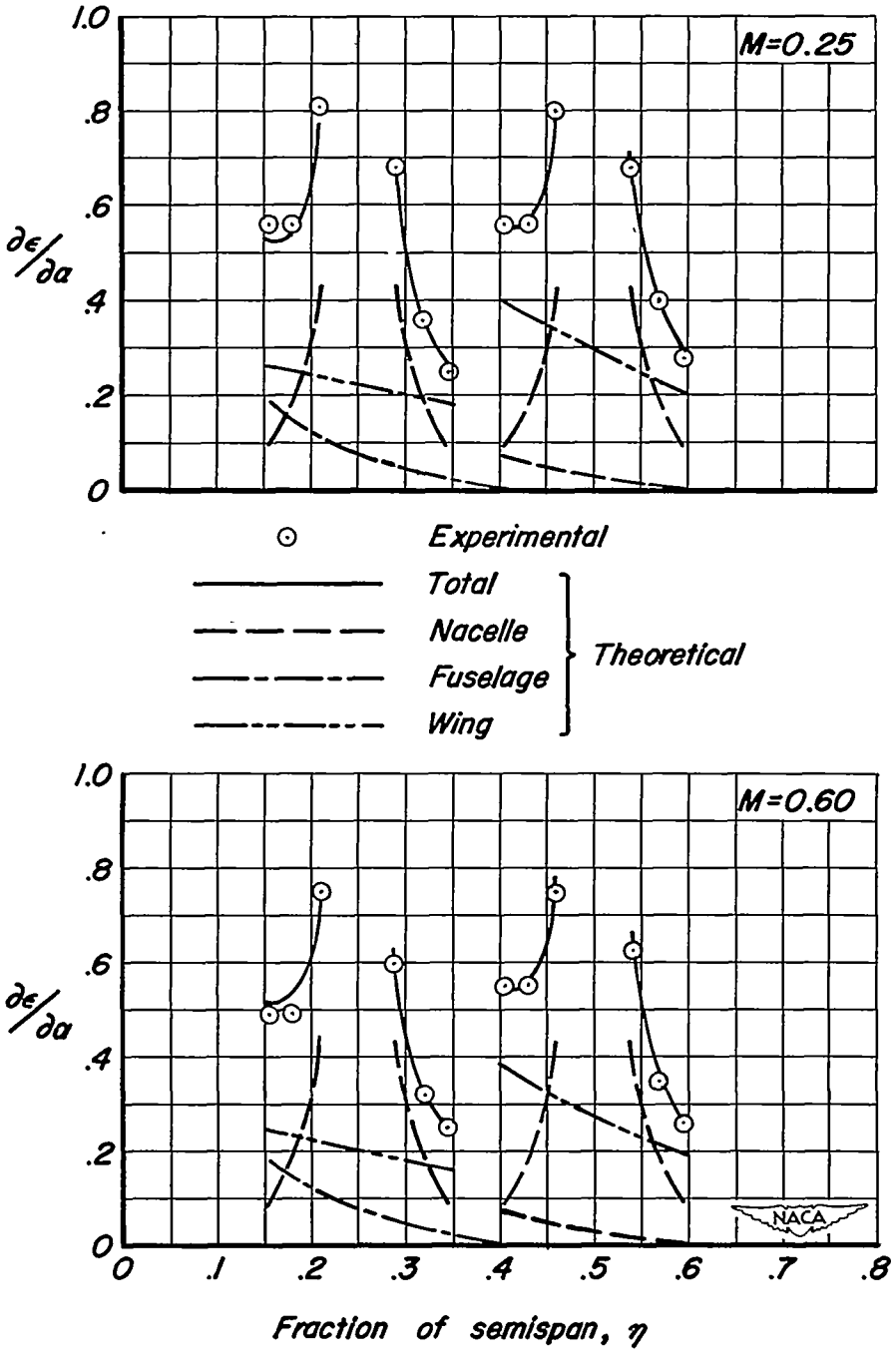

(a) M=0.25, M=0.60

Figure 6.— Spanwise variation of upwash parameter $\partial\epsilon/\partial\alpha$ at several Mach numbers.

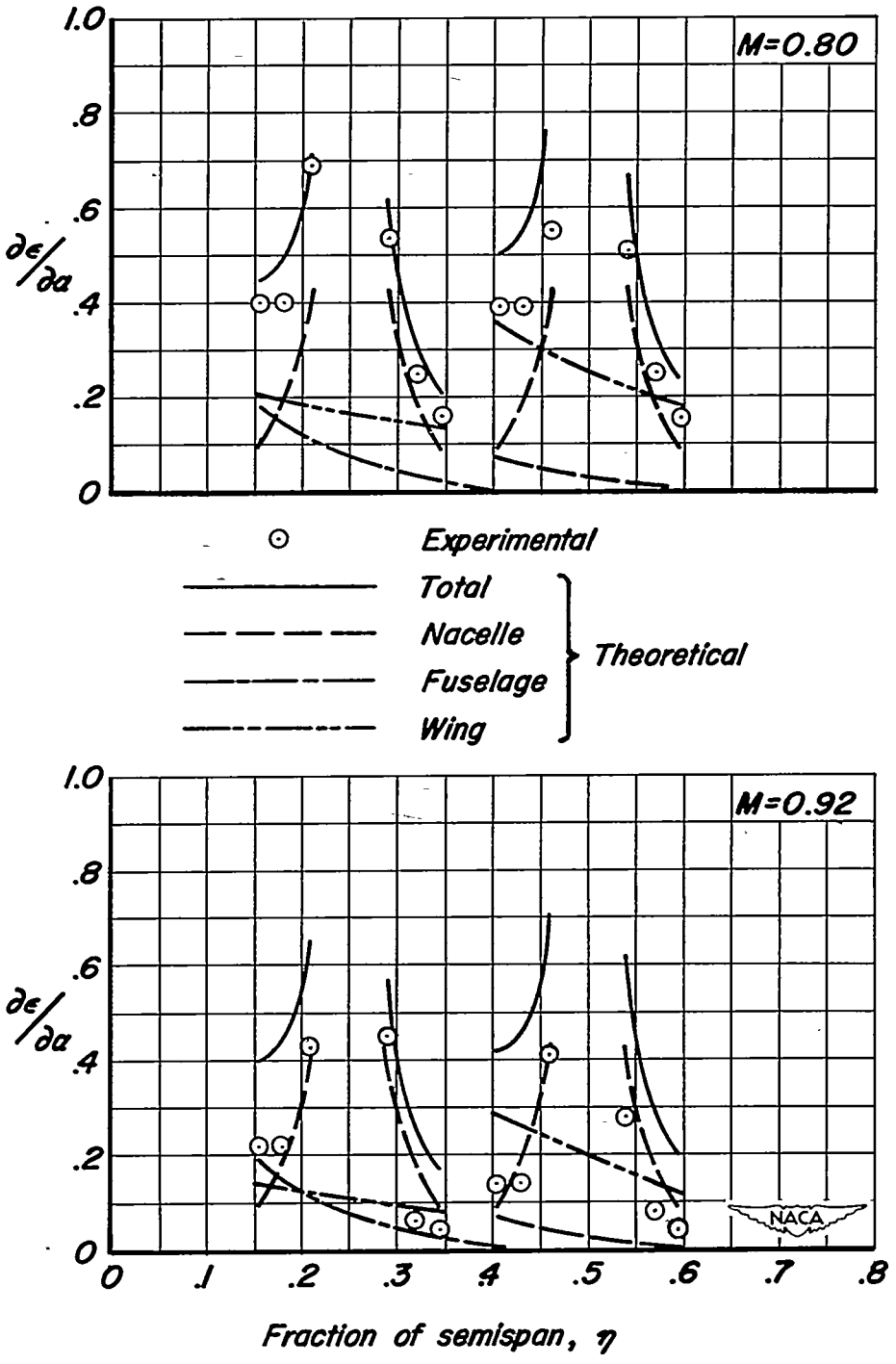

(b) M=0.80, M=0.92

Figure 6.– Concluded.

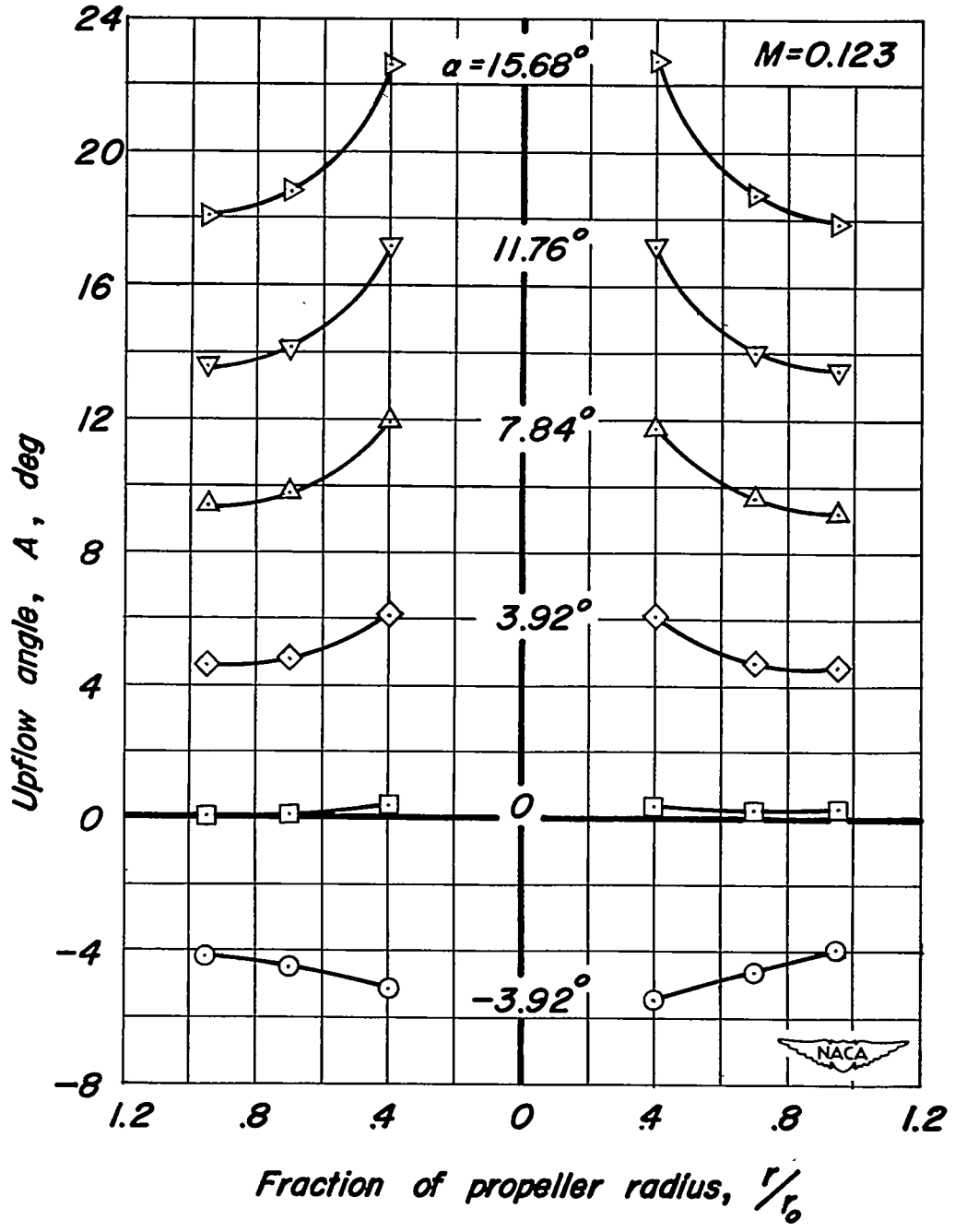

(a) M=0.123, R=4,000,000

Figure 7.– Upflow angles at various angles of attack of the nacelle alone.

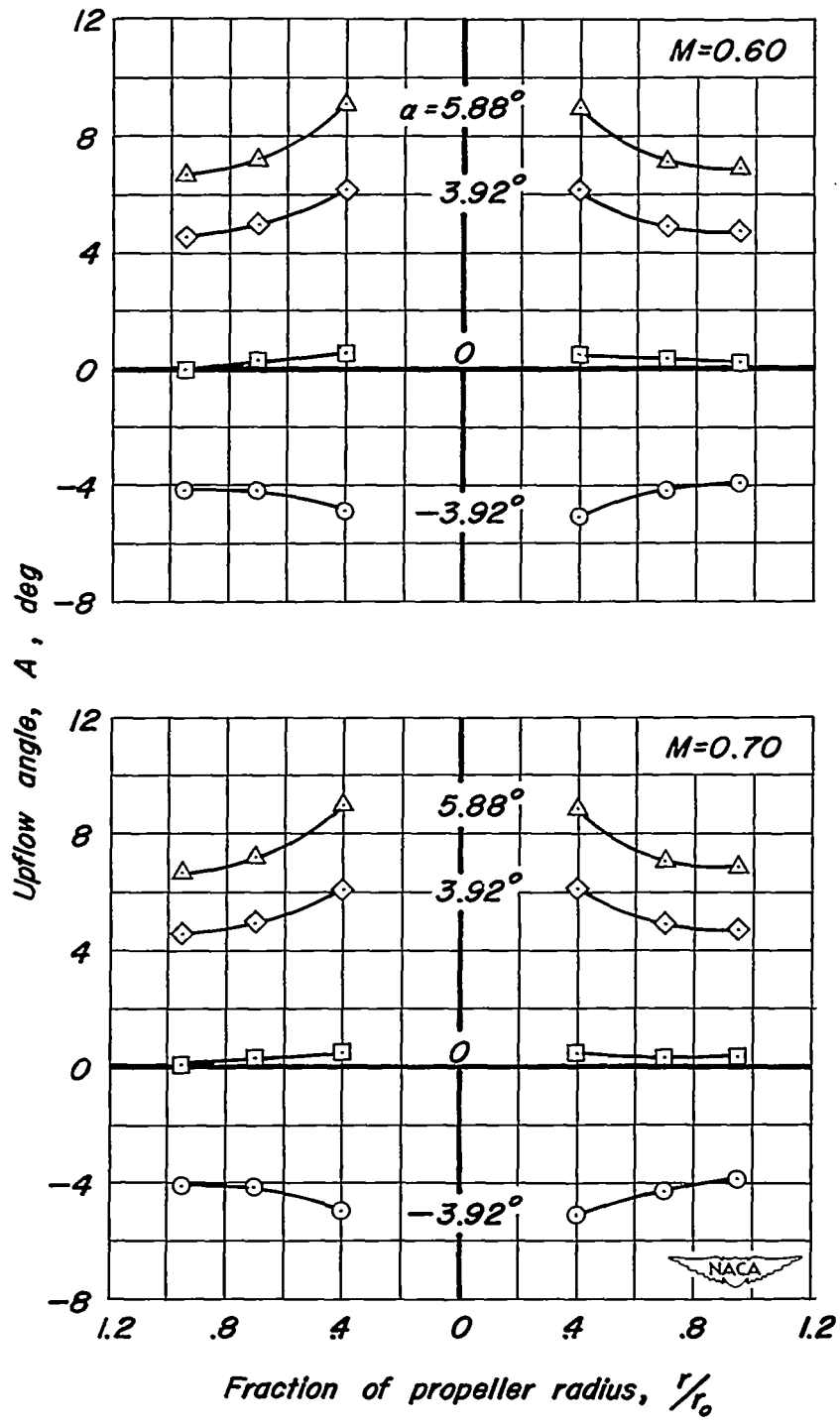

(b) M=0.60, 0.70; R=2,000,000

Figure 7.– Continued.

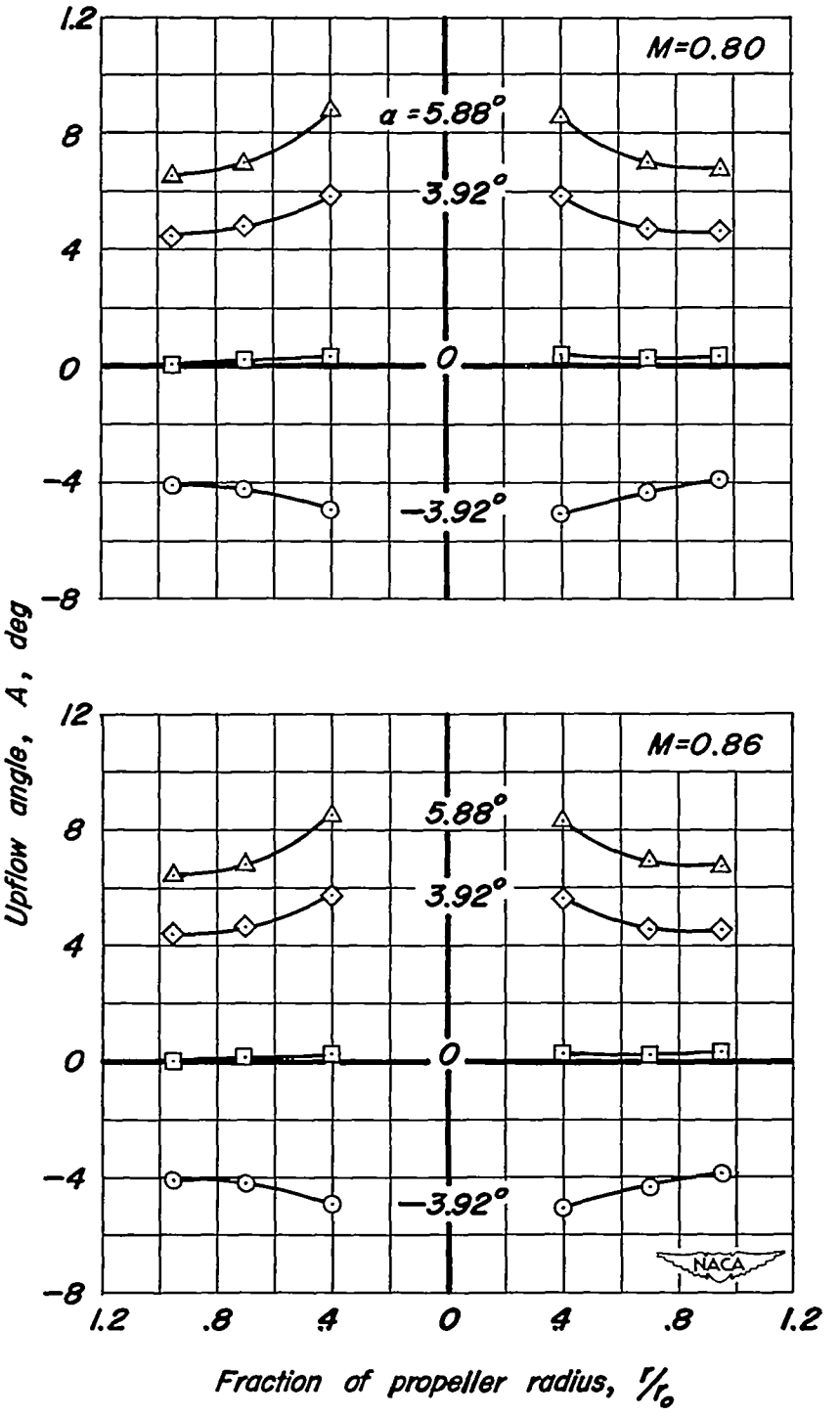

(c) M=0.80,0.86; R=2,000,000

Figure 7.– Continued.

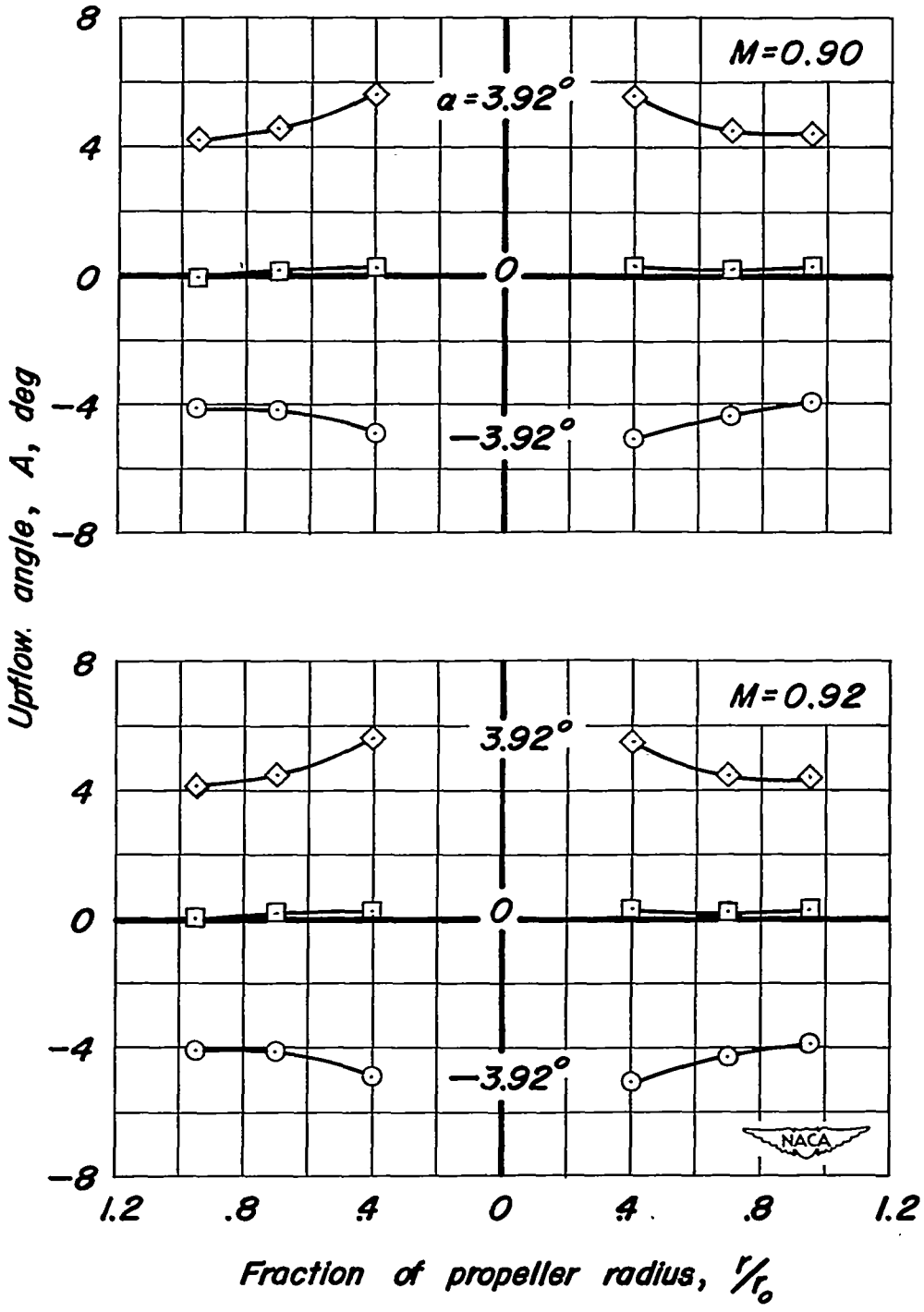

(d) M=0.90,0.92; R=2,000,000

Figure 7.—Concluded.

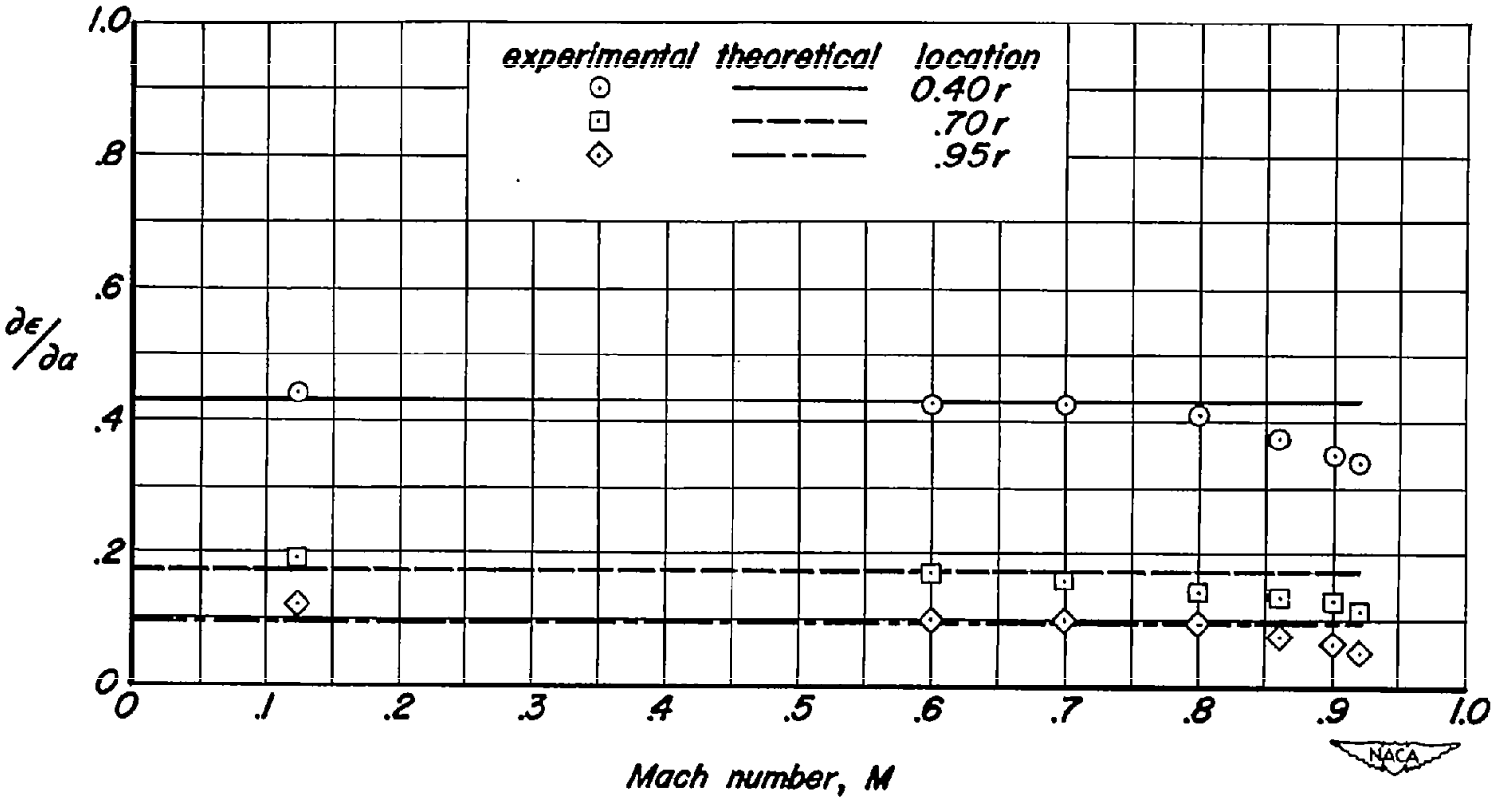

Figure 8.–Variation with Mach number of the upwash parameter $\partial\epsilon/\partial\alpha$ for the nacelle alone.

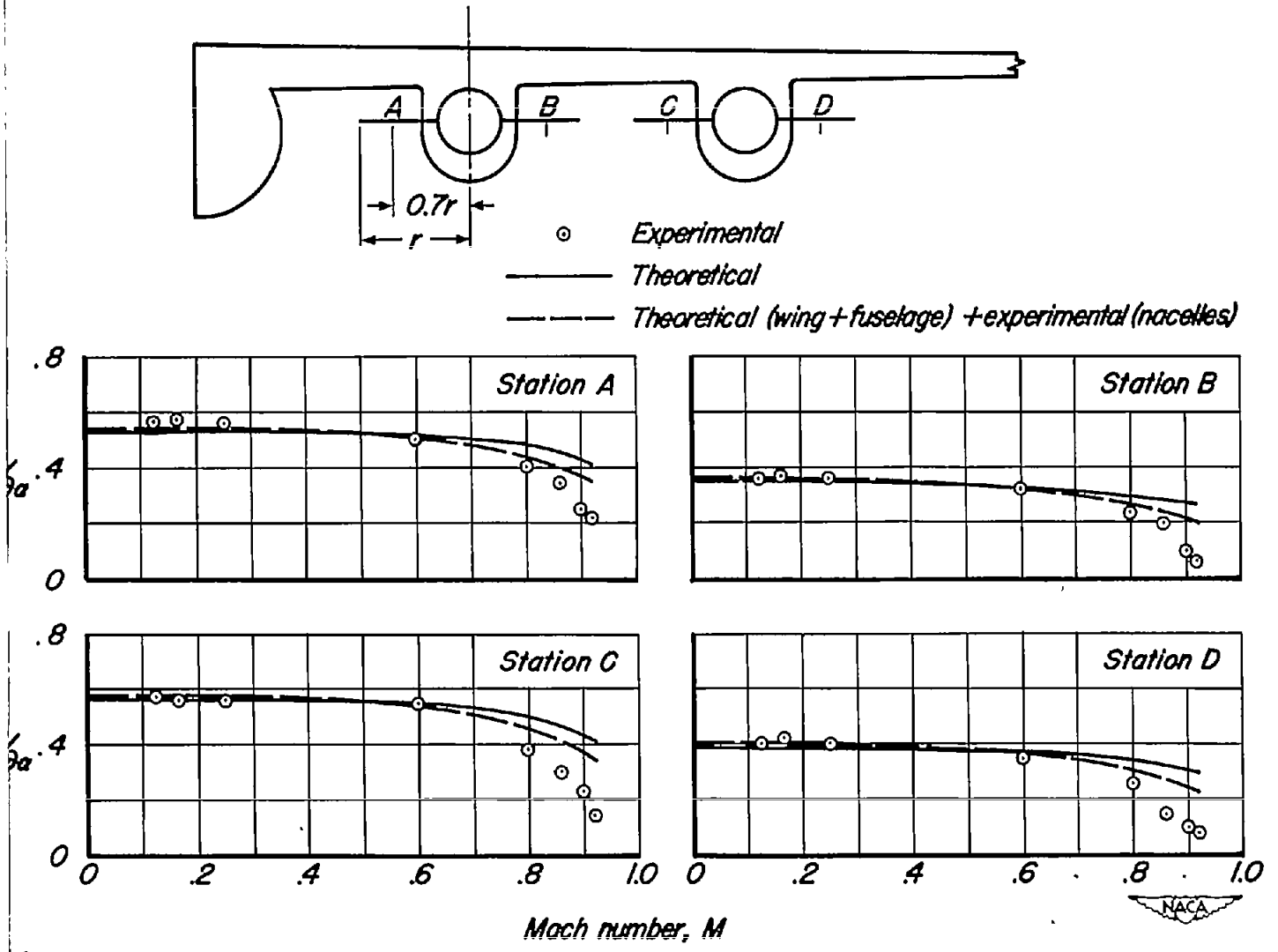

Figure 9.– Variation with Mach number of the upwash parameter $\partial\epsilon/\partial\alpha$ at 0.7 propeller radius.